Global Deep Ocean Observations of Horizontal Eddy-Mean Interactions of Temperature Variance

F. Sévellec*, N. Kolodziejczyk, A. Hochet, and T. Huck

Laboratoire d'Océanographie Physique et Spatiale, Univ Brest CNRS IRD Ifremer, Brest, France

Submitted to *J. Phys. Oceanogr.* 10 October 2025

Revised 11 February 2026 and X April 2026

* *Corresponding author address:* Laboratoire d'Océanographie Physique et Spatiale, Institut Universitaire Européen de la Mer, Technopôle Brest Iroise, Plouzané, FRANCE. Phone: +33-290-91-5540 email: florian.sevellec@univ-brest.fr

Abstract

Ocean eddies are ubiquitous in the ocean. Characterizing and quantifying their impact on the large-scale ocean circulation is key. Here we compute eddy-mean interactions for Conservative Temperature variance, including temperature variance transfers. This is done using the ANDRO dataset, which records mean temperature and horizontal displacement of Argo floats during their journey at parking depth (~1 000 m). The analysis does not show any consistency between the sign of the turbulent heat flux and the slope of the mean isotherms, questioning the validity of traditional downgradient flux turbulent closure in the context of temperature variance budget. The temperature variance interactions suggest the dominance of the non-local, redistribution term over the local, transfers term. They both have typical spatial scales ranging from 200 km to 1 000 km. When averaged over large regions, transfers are from the mean to the turbulence, but the North West Atlantic remains a unique region which acts as a turbulence graveyard. Within a water mass framework, transfers are quite consistently shrinking the mean temperature distribution except for a few extreme Water Masses: the Arctic Intermediate Water, the Antarctic Bottom Water, and the Red Sea – Persian Gulf Intermediate Water. This is also the case for a subset of the Mediterranean Water. However the Mediterranean Water is the main location of the broadening of the mean temperature distribution. These results provide observational evidence of the action of the turbulence on the mean temperature structure that could be tested in numerical ocean and climate models for validation and for the development and the implementation of ocean turbulent closures.

1 Introduction

Since the preindustrial era, climate is changing at an unrecorded pace (Eyring et al., 2016). This is true for all its components, including the ocean that has stored 90% of the heat excess (von Schuckmann et al., 2023). This heat changes the large-scale ocean temperature structure. To further anticipate this change, it becomes more and more timely to better understand the dynamics and the physical process controlling this large-scale ocean temperature structure. In parallel, one of the most energetic features, that is ubiquitous in the ocean (Chelton et al., 2007), is the mesoscale eddy turbulence (Ferrari and Wunsch, 2009). Hence understanding how this energetic turbulence and the large-scale temperature structure interact is the central question of this study.

There is a long history of studying eddy-mean flow interactions in the fields of ocean and atmospheric research. We could cite the negative viscosity concept of Starr (1968), rationalizing the eddy-driven character of the midlatitude westerlies, or the eddy-forced nature of the inertial recirculation of the Gulf Stream, established by Holland (1978) and Rhines and Holland (1979). Focusing on the temperature, it is well accepted that mean temperature gradients, through their effect on density, contribute to feed eddy turbulence through baroclinic instability (Charney, 1947; Eady, 1949). However this turbulence impacts the temperature field through isopycnal eddy diffusion (McDougall and McIntosh, 2001; McDougall et al., 2014; Groeskamp et al., 2020; Sévellec et al., 2022, 2025b). This is typical evidence of the two-way eddy-mean flow interactions for temperature. However this classical and somehow plausible description remains quite qualitative. A more analytical and robust approach to quantitatively characterize the eddy-mean interactions for temperature is thus required.

A robust framework for identifying global-average eddy-mean flow interactions has been developed by Lorenz (1955). This has been extensively used in the oceanographic community to study the interactions between the mean and the eddy Kinetic Energy (e.g., Ferrari and Wunsch, 2009). However, when applied locally, this global framework suffers from an apparent discrepancy between the local gain/loss of the mean energy reservoir and the local loss/gain of the eddy energy reservoir. This has been rationalized through the definition of a ghost reservoir (Residual Kinetic Energy) acting as a mediator between the mean and eddy Kinetic Energy (Murakami, 2011; Murakami et al., 2011; Chen et al., 2014, 2016; Kang and Curchitser, 2015; Yan et al., 2019; Matsuta and Masumoto, 2021; Jamet et al., 2022; Sévellec et al., 2025a). However these studies do not focus on tracers and are thus not directly generalizable to the temperature. Hence, in parallel to these studies there exists a wide range of studies on tracer variance budget (Sévellec et al., 2006; Arzel et al., 2006; Buckley et al., 2012; Hochet et al., 2020; Sévellec et al., 2021; Hochet et al., 2023, 2024b). This framework allows to quantitatively estimate sources and sinks of tracer variance. However these studies are not relating the mean and the eddy temperature. Hochet et al. (2024a) attempted to rationalize the link between mean reservoir gain and loss and eddy reservoir loss and gain, respectively. Whereas their suggestion is perfectly valid for global interpretation, they face the same local issue than the one discussed above for Kinetic Energy. They find an inconsistency between gain and loss of tracer variance by the mean and eddy reservoirs. Hence a consistent framework, analog to the one for Kinetic Energy and valid for local interactions but tailored for temperature, is needed.

Indeed there are specific scientific questions and challenges for the temperature budget. This could be illustrated by starting from the evolution equation for the Conservative Temperature. This reads:

$$D_t\Theta = F_\Theta + D_\Theta, \tag{1}$$

where Θ is the Conservative Temperature (McDougall and Barker, 2011), D_t is the material derivative, and F_Θ and D_Θ are the surface atmospheric forcing and small-scale dissipative terms. The material derivative reads $D_t{=}\partial_t{+}\boldsymbol{u}^\dagger \cdot \boldsymbol{\nabla}$, where t is time, $\boldsymbol{u}^\dagger{=}(u{,}v{,}w)$ is the three dimensional velocity vector (with u, v, and w being the zonal, meridional, and vertical velocities, and $\boldsymbol{\nabla}^\dagger \cdot \boldsymbol{u}{=}0$ ensure the non-divergence of the flow), $\boldsymbol{\nabla}^\dagger{=}(\partial_x{,}\partial_y{,}\partial_z)$ is the three dimensional derivative operator (with x, y, and z being the longitude, latitude, and depth), $\cdot$ is the three dimensional scalar product, and † is the transpose operator. Based on this equation and an *ad hoc* derivation using a water mass framework (Walin, 1982), Zika et al. (2015) suggested that the water masses distribution is controlled by an equilibrium between the forcing term and the dissipation. Indeed, intuitively if the dissipation term is a diffusion, by mixing waters it removes the differences and sharpens the distribution. In the case of diffusion represented by downgradient fluxes, it is indeed trivial. Hence only remains the forcing term to maintain temperature differences and broaden the distribution. This is equivalent to inflection point in Temperature-Salinity diagram due to the "stirring" of water types (i.e., temperature-salinity properties at their origin/formation). However, if one is interested by some kind of spatio-temporal average rather than local/instantaneous value, (1) would be modified to include a turbulent term. Hence all the previous neat arguments would fail if this term was not equivalent to a diffusion characterized by downgradient fluxes. For instance, if the turbulent term acts as a negative diffusivity, similarly to the so-called negative viscosity described by Starr (1968), it would broaden the temperature distribution. To clarify this, in the present study, we will derive the exact equation controlling the broadening/sharpening of spatio-temporal average ocean temperature distribution. We will then describe the impact of mesoscale turbulence for the distribution of temperature in the ocean.

To this purpose we will use the ANDRO dataset (Ollitrault and Rannou, 2013), that provides concomitant horizontal velocity and temperature observations measured during the deep displacements of Argo floats. To diagnose eddy-mean interactions with this dataset, we will develop a framework describing the interactions between the Mean Temperature Variance and the Eddy Temperature Variance. Equivalently to the description of eddy-mean flow interactions for Kinetic Energy, we will show the existence of local and non-local interactions. The former corresponds to variance transfers, whereas the latter corresponds to variance redistribution. Application of the framework to the dataset shows that the eddy turbulence tends on average to smooth mean temperature differences (as hypothesized by Zika et al., 2015), but not locally.

The manuscript is organized as follows. In section 2 the ANDRO dataset is described. In section 3 the theoretical framework is derived and restriction to an horizontal framework is discussed. The results are presented in section 4. We conclude with discussions of our results in section 5.

2 The ANDRO dataset

In this study, we have used temperature record and velocity estimations from Argo float deep displacements. By using temperature recorded during deep displacements, rather than during vertical profiles, we have consistent observations of temperature and velocities. These observations are provided by the ANDRO dataset (Ollitrault et al., 2025). In particular we used the #116520 release of 2025. It has all the Argo float deep drifts from 2000 to 2009, but is only partially complete for 2010-2025. This dataset corresponds to 1 678 510 observations, but when selecting the studied pressure range (950-1 150 dbar) we find 1 248 238 observations (Fig. 1a). In the rest of the study, we will consider this depth to be ∼1 000 m. When limiting the range of temperature between −2°C and 13°C (to avoid erroneous data), we obtained 1 221 746 observations. This leads to a mean observation density of 144.0 observations per 2°×2° with a standard deviation of 87.9 observations per 2°×2° and a maximum observation density reaching 915 observations per 2°×2° (Fig. 1b).

Using these velocity and temperature records we computed the mean of the zonal velocity, meridional velocity, and Conservative Temperature fields, on a 1°×1°-grid, as:

$$\bar{u} = \frac{1}{n}\sum_{i=1}^{n} u_i, \tag{2a}$$

$$\bar{v} = \frac{1}{n}\sum_{i=1}^{n} v_i, \tag{2b}$$

$$\bar{\Theta} = \frac{1}{n}\sum_{i=1}^{n} \Theta_i, \tag{2c}$$

where u_i and v_i are individual deep zonal and meridional velocity records, respectively, Θ_i is individual deep Conservative Temperature record, i is the index of the record, and n is the total number of records within a 2°×2° cell centered on a 1°×1° grid point.

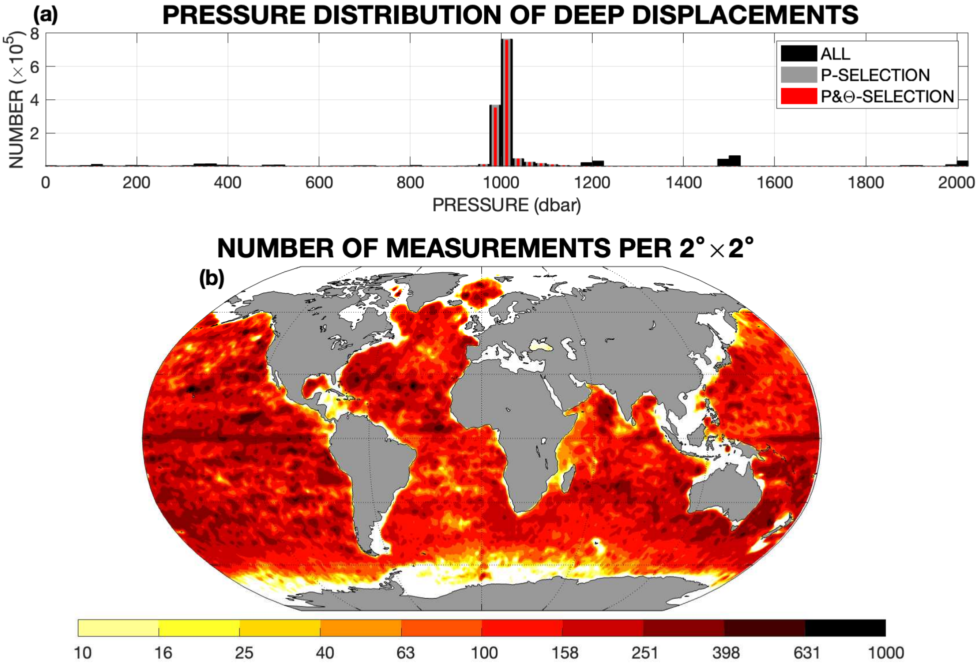

FIGURE 1: Distribution of velocity observations from the ANDRO dataset. (a) Distributions of the parking depth pressure of the Argo float deep displacements from the ANDRO dataset (#116520). Two sequential selections of observations: P-selection corresponding to a range of pressure (from 950 dbar to 1 150 dbar) and $P\&\Theta$-selection corresponding to both the range of pressure and a range of Conservative Temperature (from -2°C to 13°C). (b) Number of $P\&\Theta$-selected deep velocities observations per 2°×2°. Note the logarithmic color scale.

We can also compute the unbiased variance of these fields:

$$\overline{u'^2} = \frac{1}{n-1}\sum_{i=1}^{n}\left(u_i - \bar{u}\right)^2, \tag{3a}$$

$$\overline{v'^2} = \frac{1}{n-1}\sum_{i=1}^{n}\left(v_i - \bar{v}\right)^2, \tag{3b}$$

$$\overline{\Theta'^2} = \frac{1}{n-1}\sum_{i=1}^{n}\left(\Theta_i - \bar{\Theta}\right)^2. \tag{3c}$$

An estimation of the deep horizontal Mean and Eddy Kinetic Energy can then be obtained as MKE=$(\bar{u}^2 + \bar{v}^2)/2$ and EKE=$(\overline{u'^2} + \overline{v'^2})/2$.

Following the same principle, we define the unbiased covariance of the zonal and meridional velocity with the Conservative Temperature. This reads:

$$\overline{u'\Theta'} = \frac{1}{n-1}\sum_{i=1}^{n}\left(u_i - \bar{u}\right)\left(\Theta_i - \bar{\Theta}\right), \tag{4a}$$

$$\overline{v'\Theta'} = \frac{1}{n-1} \sum_{i=1}^{n} (v_i - \bar{v}) \left(\Theta_i - \bar{\Theta}\right). \tag{4b}$$

At 1 000 m, we find mean Conservative Temperature going from −1.8°C in the Nordic Seas to 11.8°C along the Portugal coast and in the Gulf of Aden (Fig. 2a). In the Southern Ocean we obtained water down to 0.5°C, whereas it is 2.5°C and 3.3°C in the Pacific and the Atlantic, respectively. This is consistent with state-of-the-art knowledge of descriptive oceanography (Talley et al., 2011). Following Emery (2018), we find a range of water masses at this depth: the Antarctic Bottom Water (AABW), the Circumpolar Deep Water (CDW), the Antarctic Intermediate Water (AAIW), the Mediterranean Water (MW), the Red Sea – Persian Gulf Intermediate Water (RSPGIW), the North Atlantic Deep Water (NADW), and the Arctic Intermediate Water (AIW). The temperature variance shows value of up to 3 K^2, localized in the Agulhas retroflection and return current, in the Gulf Stream and its continuation as the North Atlantic Current, in the Antarctic Circumpolar Current, and in the North Brazilian Current retroflection (Fig. 2b). In terms of momentum, the Mean and Eddy Kinetic Energy (MKE and EKE) have values of up to 10^{-2} m^2 s^{-2} and 2×10^{-2} m^2 s^{-2}, respectively. They are strong in intense western boundary currents (*e.g.*, Gulf Stream, Kuroshio, Zapiola Gyre, and Agulhas Current and its retroflection), as well as in the ACC (Fig. 2c and d). EKE is also strong in the equatorial region. This was already reported with an older version of the same dataset (#109566) by Sévellec et al. (2025a).

Using error estimates of the individual velocities provided by the ANDRO dataset (Ollitrault et al., 2025), full error estimation has been provided in Sévellec et al. (2024) and Sévellec et al. (2025a). This includes observation error (primarily controlled by the Argo float positioning error at 1000 dbar), sample size error, and error introduced by the grid-scale choice of the analysis. We refer the readers to these two studies for details. Overall, these error estimations show the robustness of analyses based on mean and variance. This directly derives from the high number of individual observations within 2°×2°-cells (Fig. 1) and the good convergence of the simple statistics, such as the mean and the variance. As in Sévellec et al. (2024) and Sévellec et al. (2025a), in the rest of the study, we will only use mean and variance. It is also worth noting that despite being Lagrangian observations the ANDRO dataset has been shown to lead to results consistent with Eulerian analyses, as for isopycnal diffusivity coefficient estimate (Sévellec et al., 2022, vs Roach et al., 2018, and Groeskamp et al., 2020), for instance.

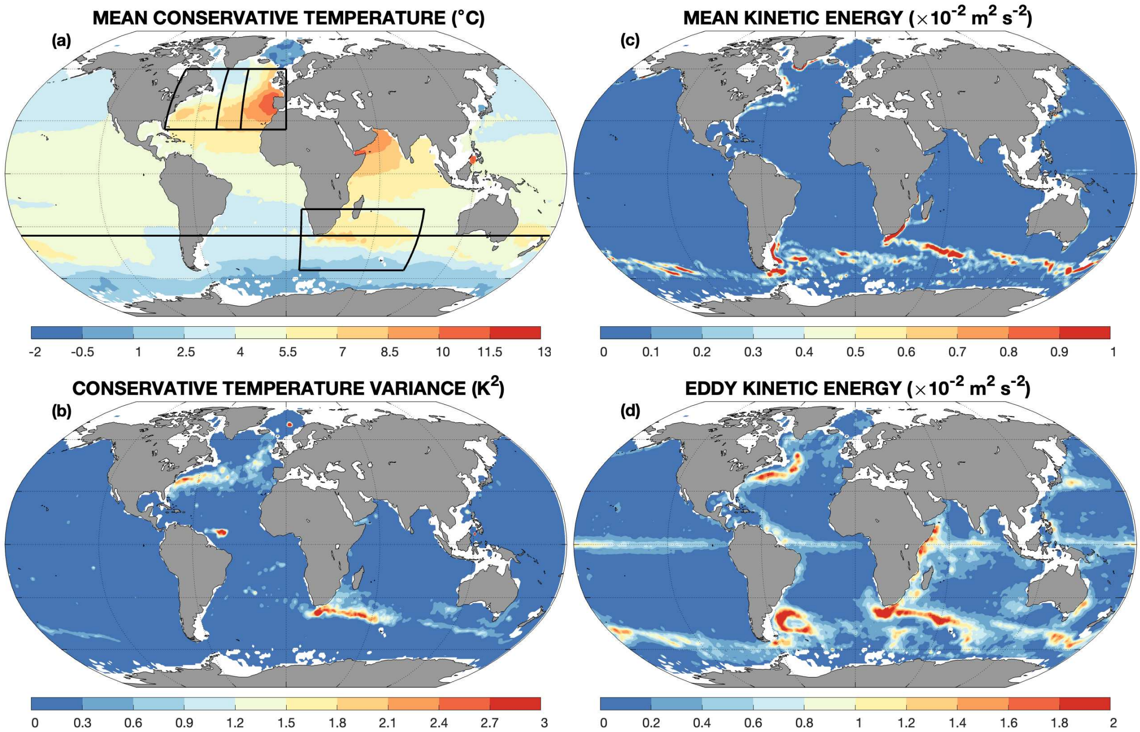

FIGURE 2: Conservative Temperature and Kinetic Energy from Argo float deep displacement observations at 1 000-m depth. (a) Mean Conservative Temperature ($\bar{\Theta}$), (b) Conservative Temperature variance ($\overline{\Theta'^2}$), (c) Mean Kinetic Energy [MKE=$(\bar{u}^2+\bar{v}^2)/2$], and (d) Eddy Kinetic Energy [EKE=$(\overline{u'^2}+\overline{v'^2})/2$]. The observations have been mapped following (2) and (3). The black line and boxes denote the regions used for spatial averages: West, Central, East, and all North Atlantic, Agulhas Current sector, and Southern Ocean sector.

3 Theoretical framework

a. *General derivations of temperature variance budget*

Restarting from (1) and applying the change of variable $T{=}\Theta{-}\langle\Theta\rangle$ (where $\langle . \rangle$ is a spatio-temporal average defined over the whole globe and over the full duration of the studied time-series), we obtain the time evolution equation for the centered temperature:

$$D_t T = F + D, \tag{5}$$

where F and D derived from F_Θ and D_Θ, respectively, but have been adapted for the change of variable. Note that $D{\equiv}D_\Theta$, if D_Θ has the form of a Laplacian. Also, note that, if the average is only a horizontal and temporal average ($\langle . \rangle_{\text{hor}}$), defining a mean stratified reference state, as often done in the context of Available Potential Energy definition (e.g, Lorenz, 1955), we have $\partial_z \langle\Theta\rangle_{\text{hor}}{\neq}0$ and the forcing F should incorporate a term of the form $-w\partial_z \langle\Theta\rangle_{\text{hor}}$ deriving from the advective term (and potentially a term deriving from the diffusive term, although it is often negligible, since the Péclet number is high – Pe$\gg$1). This property will be used in section 4d..

From (5) and splitting the temperature and velocity in a statistical mean and an anomaly so that $T{=}\bar{T}{+}T'$ and $\boldsymbol{u}{=}\bar{\boldsymbol{u}}{+}\boldsymbol{u}'$, where $\overline{T'}{=}0$ and $\overline{\boldsymbol{u}'}{=}(0{,}0{,}0)$, we obtain the evolution equation for the mean and anomalous centered temperature:

$$\partial_t \bar{T} + \boldsymbol{\nabla}^\dagger \cdot \left(\bar{\boldsymbol{u}}\bar{T}\right) = \underbrace{-\boldsymbol{\nabla}^\dagger \cdot \overline{\boldsymbol{u}'T'}}_{\mathcal{C}} + \bar{F} + \bar{D}, \tag{6a}$$

$$\partial_t T' + \boldsymbol{\nabla}^\dagger \cdot \left(\boldsymbol{u}T'\right) = -\boldsymbol{\nabla}^\dagger \cdot \left(\boldsymbol{u}'\bar{T}\right) + \underbrace{\boldsymbol{\nabla}^\dagger \cdot \overline{\boldsymbol{u}'T'}}_{-\mathcal{C}} + F' + D'. \tag{6b}$$

where $\overline{\boldsymbol{u}'T'}^\dagger{=}(\overline{u'T'}{,}\overline{v'T'}{,}\overline{w'T'})$ is the turbulent temperature flux. (Note that $T'{=}\Theta'$.) This shows the importance of the divergence of the turbulent temperature flux ($\overline{\boldsymbol{u}'T'}$) in forcing the mean temperature. This term could also be interpreted as the closure term for the large scale evolution: $\mathcal{C}{=}{-}\boldsymbol{\nabla}^\dagger \cdot \overline{\boldsymbol{u}'T'}$.

To study the variance, we define three temperature variance reservoirs: the Mean, the Residual, and the Eddy Temperature Variance reservoirs, so that MTV$=\bar{T}^2$, $\overline{\text{RTV}}{=}2\overline{\bar{T}T'}{=}0$, and $\overline{\text{ETV}}{=}\overline{T'^2}$ (Fig. 3). This decomposition directly derived from $T^2{=}\bar{T}^2{+}2\bar{T}T'{+}\overline{T'^2}$. This corresponds to the zeroth, first, and second order anomaly of the temperature square. It is worth noting that residual reservoir is identical to zero on average, and could then be considered has a "ghost" reservoir. However as shown latter, and in analogy with the work of Chen et al. (2014, 2016) in the context of Kinetic and Potential Energy, it is key as RTV acts as a mediator between ETV and MTV. From multiplying (6) with either $\bar{T}$ or T', we obtain the evolution of these three temperature variance reservoirs. This leads to:

$$\partial_t \bar{T}^2 + \boldsymbol{\nabla}^\dagger \cdot \overline{\boldsymbol{u}\bar{T}^2} = \underbrace{-2\bar{T}\boldsymbol{\nabla}^\dagger \cdot \overline{\boldsymbol{u}'T'}}_{\mathcal{R}=\mathcal{A}+\mathcal{T}} + 2\bar{T}\bar{F} + 2\bar{T}\bar{D}, \tag{7a}$$

$$\partial_t 2\underbrace{\overline{\bar{T}T'}}_{=0}+\underbrace{\boldsymbol{\nabla}^\dagger\cdot\overline{\boldsymbol{u}2\bar{T}T'}}_{-\mathcal{A}}=\underbrace{2\bar{T}\boldsymbol{\nabla}^\dagger\cdot\overline{\boldsymbol{u}'T'}}_{-\mathcal{R}}+\underbrace{2\left(\boldsymbol{\nabla}\bar{T}\right)^\dagger\cdot\overline{\boldsymbol{u}'T'}}_{\mathcal{T}}+\underbrace{2\overline{\bar{T}\left(F'+D'\right)}+2\overline{T'\left(\bar{F}+\bar{D}\right)}}_{=0}, \tag{7b}$$

$$\partial_t\overline{T'^2}+\boldsymbol{\nabla}^\dagger\cdot\overline{\boldsymbol{u}T'^2}=\underbrace{-2\left(\boldsymbol{\nabla}\bar{T}\right)^\dagger\cdot\overline{\boldsymbol{u}'T'}}_{-\mathcal{T}}+2\overline{T'F'}+2\overline{T'D'}. \tag{7c}$$

Here we find that the eddy-mean interactions, $\mathcal{R}{=}-2\bar{T}\boldsymbol{\nabla}^\dagger\cdot\overline{\boldsymbol{u}'T'}$, is the sum of the variance redistribution, $\mathcal{A}{=}-2\boldsymbol{\nabla}^\dagger\cdot\left(\bar{T}\overline{\boldsymbol{u}'T'}\right)$, and the variance transfers, $\mathcal{T}{=}2\left(\boldsymbol{\nabla}\bar{T}\right)^\dagger\cdot\overline{\boldsymbol{u}'T'}$. Following analog work done on eddy-mean flow interactions for the Kinetic Energy reservoirs (Chen et al., 2014, 2016; Sévellec et al., 2025a), we also define $\mathcal{R}$, $\mathcal{A}$, and $\mathcal{T}$ as the total, non-local, and local interactions (Fig. 3). In (7) we see the special role of advection for RTV ($\mathcal{A}$). Indeed for MTV and ETV, their respective advection only acts as an intra-reservoir action. However for RTV, because RTV is unambiguously zero on average, this intra-reservoir action impacts the inter-reservoir interactions and accumulates with $\mathcal{T}$ from ETV to impact MTV through $\mathcal{R}$.

Equivalent derivations have been done in the context of energy reservoir exchange of Available Potential Energy ($\propto\rho^2$, where ρ is density) by Kang and Curchitser (2015) and Chen et al. (2016) and of potential energy in a quasi-geostrophic model [$\propto(\partial_z\psi)^2$, where ψ is the streamfunction] by Jamet et al. (2024), for instance. These derivations lead to equivalent eddy-mean interaction terms and reservoirs.

From (7) we can retrieve the more classical global view (equivalent to the Lorenz, 1955, energy cycle) by integrating over the volume of the ocean. This reads:

$$\partial_t\iiint_V\bar{T}^2\,dv=2\iiint_V\left(\boldsymbol{\nabla}\bar{T}\right)^\dagger\cdot\overline{\boldsymbol{u}'T'}\,dv+2\iiint_V\left(\bar{T}\bar{F}+\bar{T}\bar{D}\right)\,dv, \tag{8a}$$

$$\partial_t\iiint_V\overline{T'^2}\,dv=-2\iiint_V\left(\boldsymbol{\nabla}\bar{T}\right)^\dagger\cdot\overline{\boldsymbol{u}'T'}\,dv+2\iiint_V\left(\overline{T'F'}+\overline{T'D'}\right)\,dv, \tag{8b}$$

where V is the total ocean volume and dv is the volume element. Here we only need two reservoirs: the global-mean MTV and ETV. Also, beyond forcing and dissipation, only the eddy-mean interactions remain, since advection terms vanish when globally averaged (as a consequence of mass conservation). Finally, the eddy-mean interactions simplify to $\iiint_V\mathcal{R}\,dv{=}\iiint\mathcal{T}\,dv$, since $\iiint_V\mathcal{A}\,dv{=}0$ (again, as a consequence of mass conservation), leading to non-ambiguous variance transfers between the mean and the eddy reservoirs. Also $\iiint_V\mathcal{R}\,dv$ is a direct contributor to the variance of the temperature distribution, showing the impact of the turbulence on the temperature distribution. Indeed dividing by the global volume, (8a) becomes an equation for the spatial-variance of the large-scale temperature ($\sigma^2_{\bar{T}}{=}\langle\bar{T}^2\rangle$). This reads:

$$\partial_t\sigma^2_{\bar{T}}=\langle\mathcal{T}\rangle+2\left\langle\bar{T}\bar{F}\right\rangle+2\left\langle\bar{T}\bar{D}\right\rangle. \tag{9}$$

This derivation was also provided in the context of freshwater content variation of the Arctic by Hochet et al. (2024a), for instance. In this expression, the forcing term acts as the

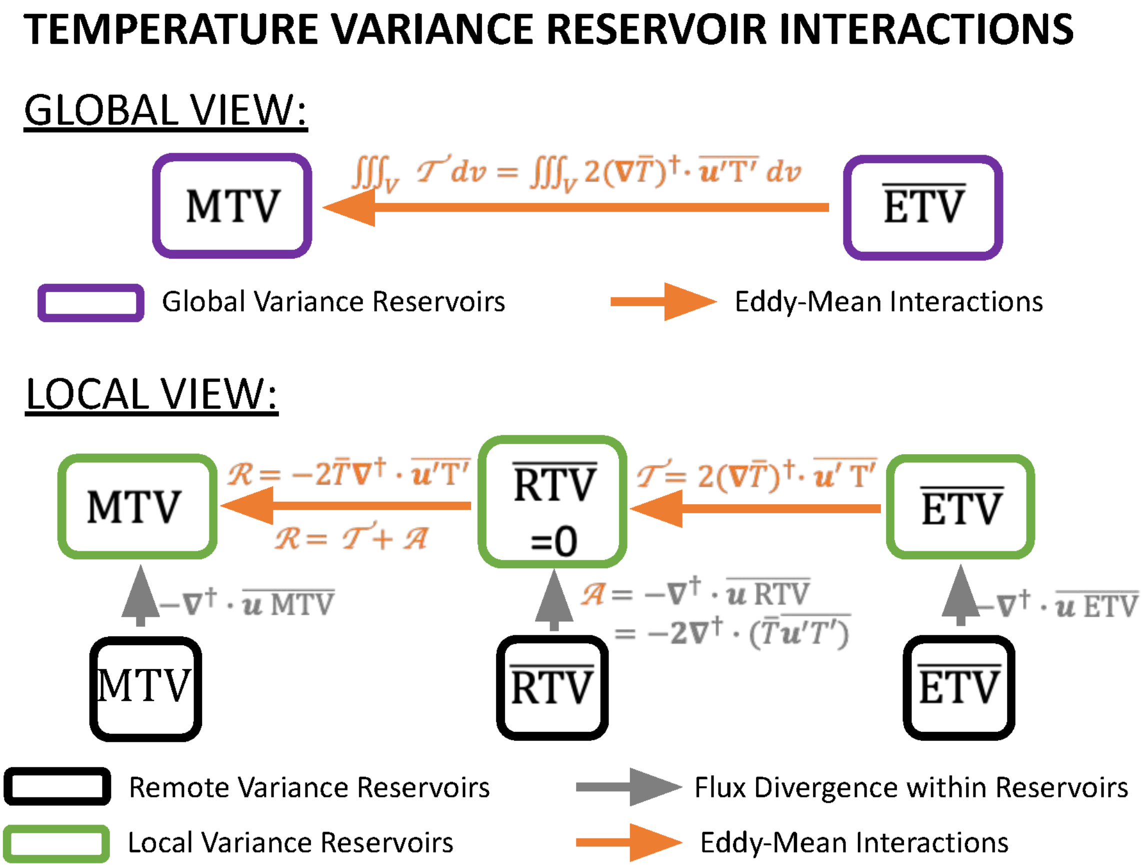

FIGURE 3: Schematic of global and local interactions between temperature variance reservoirs. Globally, variance transfers are from Eddy Temperature Variance ($\overline{\mathrm{ETV}}$=$\overline{T'^2}$) to Mean Temperature Variance (MTV=$\bar{T}^2$) through the intra-reservoir action of the spatial integral of the eddy-mean interactions, solely controlled by the local component (*i.e.*, $\iiint_V \mathcal{R}\,dv$=$\iiint_V \mathcal{T}\,dv$). Locally, variance transfers occur both through the intra-reservoir action of advection and through the inter-reservoir action of the eddy-mean interactions. Here, the reservoirs are the Mean Temperature Variance (MTV=$\bar{T}^2$), the Residual Temperature Variance ($\overline{\mathrm{RTV}}$=$2\overline{\bar{T}T'}$=0), and the Eddy Temperature Variance ($\overline{\mathrm{ETV}}$=$\overline{T'^2}$). The eddy-mean interactions correspond to the total component ($\mathcal{R}$) received by Mean Temperature Variance, the local component ($\mathcal{T}$) leaving the mean Eddy Temperature Variance, and the non-local component ($\mathcal{A}$) leaving the mean Residual Temperature Variance and ensuring that it remains zero at all time despite the existence of RTV eddy-advection. By construction the total component is the sum of the local and non-local components ($\mathcal{R}$=$\mathcal{A}$+$\mathcal{T}$).

spatial-covariance between temperature forcing and the mean temperature field. Hence, beyond the amplitude, the shape consistency between the temperature forcing and the mean temperature, is key in modifying the spatial-variance of the large-scale temperature.

At high Péclet number (Pe$\gg$1 – diffusion is negligible over advection: $\langle \bar{T}\bar{D}\rangle \simeq 0$) the distribution is maintained (i.e., $\partial_t \sigma^2_{\bar{T}}$=0) by a balance between the forcing and the action of the turbulence:

$$\langle \bar{T}\bar{F}\rangle = -\frac{1}{2}\langle \mathcal{T}\rangle . \tag{10}$$

This is the analytical demonstration of the intuitive description of the maintenance and broadening of the ocean's tracer distribution suggested by Zika et al. (2015), who only proposed an advanced scaling argument.

Even if not of leading order locally (i.e., Pe$\gg$1), it is possible that the global impact of the diffusive term is key. The small-scale dissipative term is often assumed to take the form of a downgradient flux Fick's law (Redi, 1982): $D = \boldsymbol{\nabla}^\dagger \cdot \left(\mathbf{K}\cdot\boldsymbol{\nabla}\bar{T}\right)$, where $\mathbf{K}$ is the diffusivity tensor. This diffusivity tensor is positively defined as it measures the spread in time of Lagrangian trajectories (Batchelor, 1949; Sévellec et al., 2022), which can only grow statistically. In this case it can be shown that the global impact of this term on the mean temperature variance reads:

$$\langle \bar{T}\bar{D}\rangle = \frac{1}{V}\iiint_V \bar{T}\boldsymbol{\nabla}^\dagger\cdot\left(\mathbf{K}\cdot\boldsymbol{\nabla}\bar{T}\right)\,dv = \underbrace{\frac{1}{2V}\oiint_\Sigma \boldsymbol{\eta}^\dagger\cdot\left(\mathbf{K}\cdot\boldsymbol{\nabla}\bar{T}^2\right)\,d\sigma}_{=0}\underbrace{-\frac{1}{V}\iiint_V \left(\boldsymbol{\nabla}\bar{T}\right)^\dagger\cdot\mathbf{K}\cdot\left(\boldsymbol{\nabla}\bar{T}\right)\,dv}_{\leq 0},$$

where Σ is the surface bounding the ocean, $d\sigma$ is its surface ocean boundary element, and $\boldsymbol{\eta}$ is the vector normal to this surface. Given that the forcing has been explicitly expressed through F, the variance flux is zero. Since it is a scalar product using a positive definite tensor, the second term is unequivocally lower than or equal to zero at all locations: $-\left(\boldsymbol{\nabla}\bar{T}\right)^\dagger\cdot \mathbf{K}\cdot\left(\boldsymbol{\nabla}\bar{T}\right)\leq 0$, and so also when globally averaged. Hence, here, we demonstrate that, under the Fick's law assumption, the small-scale dissipative term leads to the shrinking of the mean temperature distribution ($\partial_t\sigma^2_{\bar{T}}\leq 0$), as also suggested by Zika et al. (2015) in a water mass transformation framework. Physically, this means that the diffusion is mixing water until there only exists a single temperature class.

Equivalently to the variance of the mean temperature, we can define the mean variance of the anomaly: $\langle\sigma^2_{T'}\rangle = \langle\overline{T'^2}\rangle$. Using (8b), its evolution is described by:

$$\partial_t\langle\sigma^2_{T'}\rangle = -\langle\mathcal{T}\rangle + 2\langle T'F'\rangle + 2\langle T'D'\rangle . \tag{11}$$

This equation has already been derived in the context of the large-scale ocean variability by Sévellec et al. (2006), for instance. The same properties can be derived for this mean variance as for the variance of the mean. (1) The forcing acts through the global mean of the correlation between forcing anomaly and the temperature anomaly. (2) Small-scale dissipation can only be a sink of variance if one assumes a downgradient flux closure: $\langle T'D'\rangle = -\langle (\boldsymbol{\nabla} T')^\dagger \cdot \mathbf{K} \cdot (\boldsymbol{\nabla} T')\rangle \leq 0$. However, scaling analysis suggests that $\langle \mathcal{T}\rangle \sim \lambda^{-1}$ and $\langle T'D'\rangle \sim \lambda^{-2}$, where λ is the typical length-scale of the studied process. Hence, for small scale processes, diffusion can become of order one (Pe$\simeq$1) or even leading order (Pe$>$1). This means that at equilibrium (i.e., $\partial_t \langle \sigma^2_{T'}\rangle = 0$) the small-scale dissipative term plays a role in the balance of the mean variance of the anomaly.

b. *Restriction to a horizontal framework*

Since we only have access to horizontal velocity (section 2) we restrict our study to horizontal interactions and adapt the general derivations of section 3a.. First we redefine T as the difference between the observed temperature and its horizontal global mean. With this definition T is the departure from the mean at $\sim$1 000 m, showing regions warmer and colder than the mean and thus the spatial structure of the temperature at this depth. In this context it is similar to the Available Potential Energy (APE, Lorenz, 1955), where for our reference depth, there is regions with higher and lower density (colder and warmer) and so higher and lower APE, respectively. For the impact of turbulent flow on the mean temperature we have only $\mathcal{C}|_{\text{hor}} = -\boldsymbol{\nabla}_H^\dagger \cdot \overline{\boldsymbol{u}'_H T'}$, where $\boldsymbol{u}_H^\dagger = (u,v)$ is the two dimensional horizontal velocity vector, $\boldsymbol{\nabla}_H^\dagger = (\partial_x, \partial_y)$ is the two dimensional horizontal derivative operator, and $\cdot$ now represents the two dimensional scalar product.

For the impact on the temperature variance within a horizontal restricted framework we obtain:

$$\mathcal{R}|_{\text{hor}} = -2\bar{T}\boldsymbol{\nabla}_H^\dagger \cdot \overline{\boldsymbol{u}'_H T'}, \tag{12a}$$

$$\mathcal{A}|_{\text{hor}} = -2\boldsymbol{\nabla}_H^\dagger \cdot \left(\bar{T}\overline{\boldsymbol{u}'_H T'}\right), \tag{12b}$$

$$\mathcal{T}|_{\text{hor}} = 2\left(\boldsymbol{\nabla}_H \bar{T}\right)^\dagger \cdot \overline{\boldsymbol{u}'_H T'}. \tag{12c}$$

Key properties of the eddy-mean interactions still remain even when focusing on the horizontal components, though. Hence, when globally averaged the horizontal component of the non-local eddy-mean interaction component reads:

$$\iint_S \mathcal{A}|_{\text{hor}}\, ds = -2\iint_S \boldsymbol{\nabla}_H^\dagger \cdot \left(\overline{\boldsymbol{u}'_H T'}\bar{T}\right)\, ds = -2\oint_L \overline{\left(\boldsymbol{n}^\dagger \cdot \boldsymbol{u}'_H\right) T'}\bar{T}\, dl = 0, \tag{13}$$

where S and L define the ocean surface and boundary at the studied depth, respectively, ds and dl define their surface and length elements, and $\boldsymbol{n}$ is the vector normal to the boundary. Hence, $\boldsymbol{n}^\dagger \cdot \boldsymbol{u}'_H$ is the projection of the horizontal turbulent flow on normal-boundary vector, which is 0 because of mass conservation (*i.e.*, no mass is transported through the boundary). This means that, even when focusing on the horizontal component, the global average of the non-local component is still 0: there is no net global eddy transport of residual temperature variance. As a consequence, the local and total components become equal:

$$\iint_S \mathcal{R}|_{\text{hor}}\, ds = \iint_S \mathcal{T}|_{\text{hor}}\, ds. \tag{14}$$

Hence, even when focusing on the horizontal components, loss and gain of mean variance are exactly equivalent to gain and loss of eddy variance, allowing the unequivocal interpretation of total/local global-mean components as variance transfers. As a global average, this term is the forcing term of the spatial variance of the mean temperature field. It shows how the turbulent flux maintains or destroys, depending of the sign, the large-scale structure of the conservative temperature. Hence it measures the ability of the turbulence to broaden or sharpen the conservative temperature distribution.

The reason for only focusing on the horizontal components of the transfers is a direct consequence of the dataset limitation. However we can still estimate the relative error of this constraint. Colin de Verdière and Tailleux (2005) and Sévellec and Huck (2016) have suggested the existence of an adimensional number (ϵ) that measures the ratio of the horizontal advection to the vertical one. It derives from the advection equation of neutral density under the assumptions of geostrophic and hydrostatic balances. This reads:

$$\epsilon = \left| \frac{f}{h\beta} \frac{\|\boldsymbol{\nabla}_H \gamma\|}{\partial_z \gamma} \right|, \tag{15}$$

where γ is the neutral density, f is the Coriolis parameter, $\beta{=}\partial_y f$ is the meridional variation of the Coriolis parameter due to the Earth's curvature, $\|\boldsymbol{\nabla}_H \gamma\|{=}\sqrt{(\boldsymbol{\nabla}_H \bar{\gamma})^\dagger \cdot (\boldsymbol{\nabla}_H \bar{\gamma})}$ is the neutral density horizontal gradient amplitude, and h is the pycnocline depth. The relative importance of horizontal and vertical advection has been reinterpreted by Sévellec and Huck (2015). They suggest the dominance of baroclinic instabilities in the horizontal "regime" ($\epsilon{\gg}1$) and the dominance of baroclinic Rossby waves in the vertical "regime" ($\epsilon{\ll}1$).

To estimate ϵ we have used the ISAS17 product (Kolodziejczyk et al., 2023) which provides temperature and salinity gridded fields from an Optimal Interpolation (Bretherton et al., 1976; Gaillard et al., 2016) of Argo profiles. The neutral density was computed through the Gibbs SeaWater Oceanographic Toolbox of TEOS-10 code. The estimation of the depth of the pycnocline was based on a scaling argument (i.e., typical depth of the pycnocline). Also, studied turbulent processes are necessarily reaching the depth of the measurement. Hence we set $h{=}1\,000$ m.

Computing the adimensional number ϵ (Fig. 4), we find that the horizontal regime is dominant poleward of the mid-latitudes (i.e., north of 35°N and south of 35°S). In particular the ACC is largely in this horizontal regime, whereas the Gulf Stream and its eastward continuation as the North Atlantic Current, the Kuroshio, the Agulhas Current, and the Zapiola Gyre are marginally but still in this horizontal regime. On the other hand subtropical and equatorial regions are in the vertical regime. (Note that the scaling is not informative at the equator because the geostrophic balance is invalid there.) As it will be shown later, this suggests that key regions for turbulent temperature flux, for mean temperature gradient, and for eddy-mean interactions are primarily within horizontal regime.

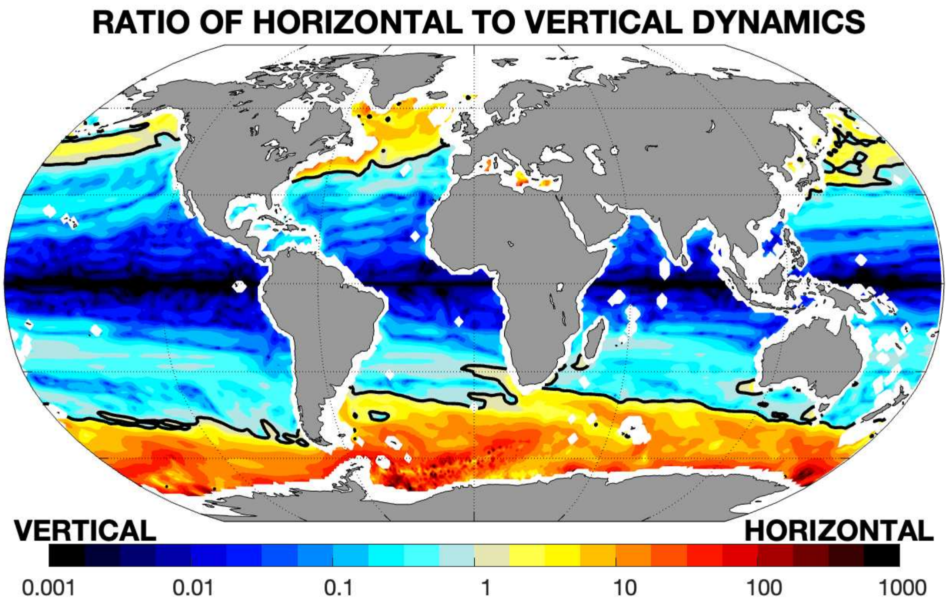

FIGURE 4: Ratio of horizontal to vertical dynamics in log scale, following (15). The ratio (ϵ) measures the propensity of the advection equation to be dominated by horizontal advection ($\epsilon \gg 1$) or by vertical advection ($\epsilon \ll 1$) under the geostrophic balance assumption. The former regime is more inductive to baroclinic instabilities, whereas the latter regime is more inductive to baroclinic Rossby waves. The thick black contour corresponds to the perfect balance (i.e., ϵ=1).

Beyond this dynamical regime argument, it is worth noting that, in our framework, part of the temperature stratification has been included in a background reservoir (by removing $\langle\Theta\rangle_{\rm hor}$). Hence it is not acting, *per se*, within the temperature interaction terms, but as a background source for the mean temperature variance. This further limits the importance of the vertical motion as it is restricted to $w\partial_z T$, instead of $w\partial_z \Theta$. The difference ($\partial_z \langle\Theta\rangle_{\rm hor}$) is fully acknowledged in our framework and will be used later to estimate the optimal vertical velocity (see section 4d.).

4 Results

a. *Data properties*

Based on the previous section, rather than focusing on zonal and meridional components, we define the turbulent temperature fluxes with respect to the Conservative Temperature horizontal gradient. Looking at the gradient amplitude ($\left\|\boldsymbol{\nabla}_H\bar{T}\right\|$), we find that it is intense along intense currents (Fig. 5). We can identify the regions of western boundary currents, such as the Gulf Stream and the Kuroshio, as well as of the ACC. An important temperature gradient is also visible in the Eastern part of the North Atlantic. This is created by the Mediterranean Water as it spreads into the cooler North Atlantic. Averaged over our 2°-cells, we find values of the mean temperature gradient of the order of several 10^{-6} K m^{-1} and up to 4×10^{-5} K m^{-1}.

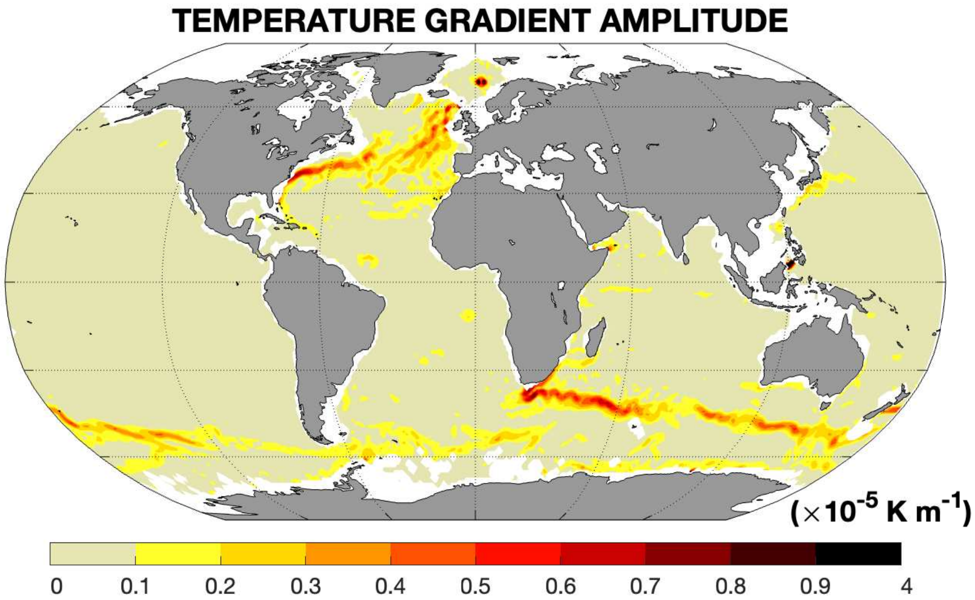

FIGURE 5: Amplitude of the horizontal mean temperature gradient ($\left\|\boldsymbol{\nabla}_H\bar{T}\right\|$).

Based on this mean temperature gradient we compute the turbulent flux along and across isotherms. This reads:

$$\overline{\boldsymbol{u}'_H T'}\Big|_{\parallel} = \overline{\boldsymbol{u}'_H T'} \times \frac{\boldsymbol{\nabla}_H\bar{T}}{\left\|\boldsymbol{\nabla}_H\bar{T}\right\|}, \tag{16a}$$

$$\overline{\boldsymbol{u}'_H T'}\Big|_{\perp} = \overline{\boldsymbol{u}'_H T'}^{\dagger} \cdot \frac{\boldsymbol{\nabla}_H\bar{T}}{\left\|\boldsymbol{\nabla}_H\bar{T}\right\|}, \tag{16b}$$

where $\times$ is the two dimensional vector product, and $\parallel$ and $\perp$ denote the along and across isothermal directions, respectively. We find that the two components are both important (Fig. 6). This means that there is turbulent fluxes both across and along the mean-temperature gradient. These fluxes reach values from a few to several 10^{-2} K m s^{-1} with a maximum absolute value of 0.15 K m s^{-1}. Focusing on the along isothermal component, we find consistent patterns that are elongated along isotherms. They are particularly strong along the Gulf Stream, the Kuroshio, and the ACC. For all three of these currents the along-isothermal turbulent flux corresponds to a positive term to the south and negative term to the north of the mean temperature gradient amplitude maximum (Fig. 5). Focusing on the across isothermal component, while the most intense patterns are still in intense boundary current and within the ACC, they also exist in the East North Atlantic (at the edge between the Mediterranean Water and the North Atlantic Deep Water). This region is quite consistently negative. Only 55% of the cross-isothermal turbulent temperature flux is Θ-downgradient (i.e., $\overline{\boldsymbol{u}_H'T'}\big|_\perp<0$). This suggests that typical diffusivity closure (i.e., Fick's law, Redi, 1982) will miss almost half of the fluxes if reconstructed by down-gradient flux of mean temperature. Note that this is potentially not problematic for the mean-temperature evolution [i.e., $\mathcal{C}$ in (6)], as only the divergent part of the flux is key (Appendix, Marshall and Shutts, 1981; Fox-Kemper et al., 2003). Following the same principle, we find that only 46% of the cross-isopycnal turbulent temperature flux is γ-downgradient (i.e., $\overline{\boldsymbol{u}_H'T'}\cdot\boldsymbol{\nabla}_H\bar{\gamma}/\left\|\boldsymbol{\nabla}_H\bar{\gamma}\right\|<0$). Overall, turbulent fluxes appear strong within regions of intense currents.

To estimate the impact of the turbulent flux onto the mean-temperature evolution we compute its divergence (i.e., $\mathcal{C}|_{\text{hor}}=-\boldsymbol{\nabla}_H^\dagger\cdot\overline{\boldsymbol{u}_H'T'}$). We find that the fluxes are of the order of several 10^{-8} K s^{-1} ($\sim$1 K in 3 years), with a maximum absolute value of 5×10^{-7} K s^{-1} (Fig. 7). The divergence of the turbulent flux occurs mainly within intense boundary currents and shows a succession of positive and negative values corresponding to warming and cooling of the mean-temperature by the turbulence, respectively. The typical spatial-scale corresponds to consistent pattern of a few to several degrees.

To estimate regional impacts of the flux divergence we compute its mean globally and over 6 active regions: the whole North Atlantic – 80°W-0° and 25°N-60°N, the Western North Atlantic – 80°W-46°W and 25°N-60°N, the Central North Atlantic – 46°W-30°W and 25°N-60°N, the Eastern North Atlantic – 30°W-0° and 25°N-60°N, the Agulhas Current sector – 10°E-90°E and 55°S-20°S, and the Southern Ocean sector – south of 35°S (as shown in Fig. 2a). This shows that the regional effect depends on the region considered (Tab. 1). At the studied depth, globally the turbulence tends to warm the mean temperature by 3.9×10^{-11} K s^{-1} ($\sim$1 K per millenia). This warming tendency is also true for the whole North Atlantic and its Western sub-region. The turbulence of the western North Atlantic leads to a warming of $\sim$1 K per century. It is the most intense average temperature changes that we have identified over the 6 tested regions. Indeed, the Central North Atlantic is more neutral, with only a slight warming on average (100 times as low as the West North

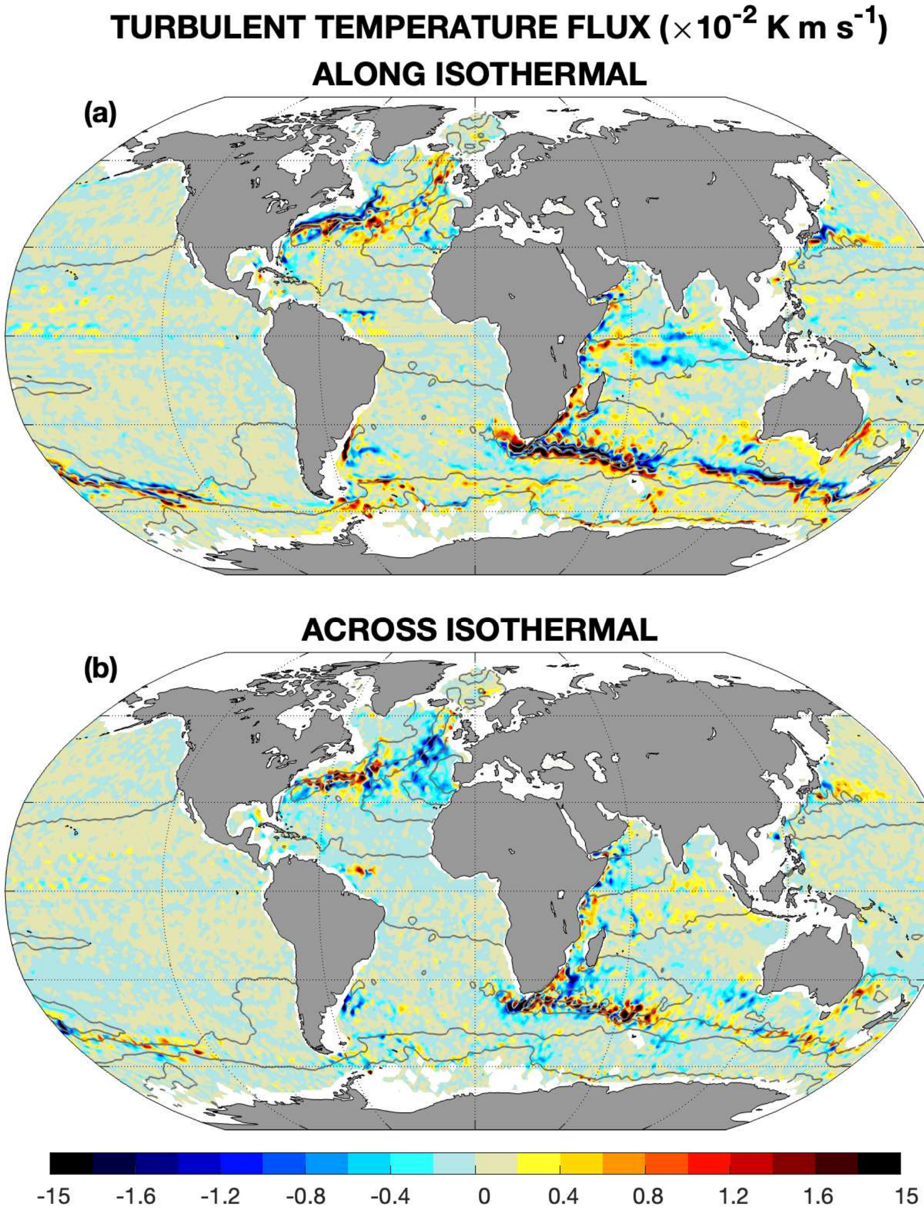

FIGURE 6: Horizontal turbulent temperature flux. Flux projected (a) along conservative isotherms ($\overline{\boldsymbol{u}'_H T'}\Big|_{\parallel}$) and (b) across conservative isotherms ($\overline{\boldsymbol{u}'_H T'}\Big|_{\perp}$), following (16). Contours show mean Conservative Temperature with contours from $-2°$C to $13°$C with $1.5°$ contour interval.

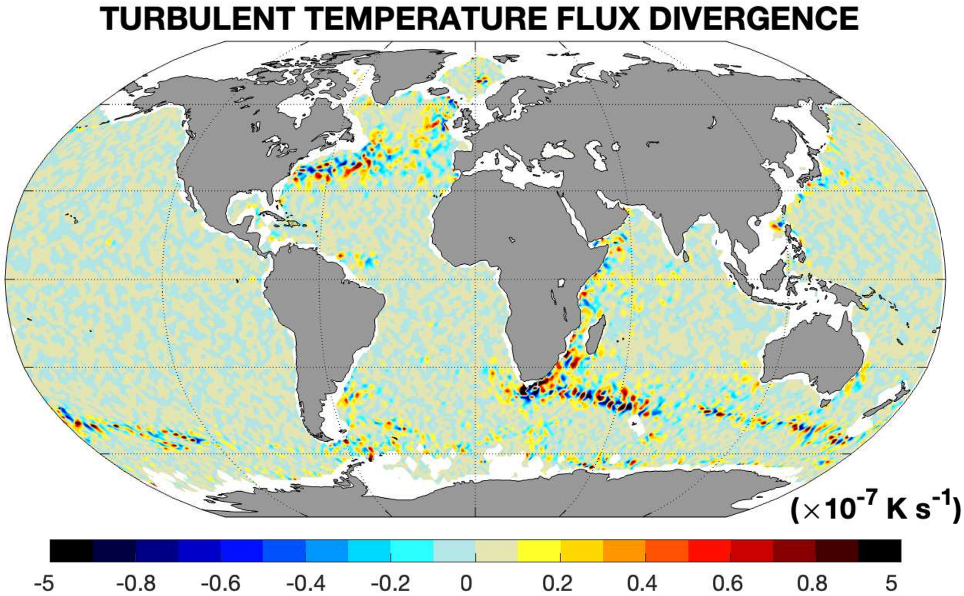

FIGURE 7: Horizontal divergence of the horizontal turbulent temperature flux ($\mathcal{C}|_{\text{hor}}{=}-\boldsymbol{\nabla}_H^{\dagger}\cdot\overline{\boldsymbol{u}'_H T'}$). This term corresponds to the horizontal components of the closure term (*i.e.*, the impact of the turbulence) for the mean temperature, following (6a).

Atlantic). On the other hand, turbulence in the east North Atlantic, the Agulhas sector, and the Southern Ocean sector all tends to cool the mean temperature. It is the most intense in the Southern Ocean sector, with an average cooling of $\sim$1 K per 150 years.

TABLE 1: Spatial-averages of turbulent temperature flux divergence both at global and regional level ($\mathcal{C}|_{\text{hor}}{=}-\boldsymbol{\nabla}_H^{\dagger}\cdot\overline{\boldsymbol{u}'_H T'}$). The 6 regions (Fig. 2a) correspond to: the whole North Atlantic (80°W-0° and 25°N-60°N), the Western North Atlantic (80°W-46°W and 25°N-60°N), the Central North Atlantic (46°W-30°W and 25°N-60°N), the Eastern North Atlantic (30°W-0° and 25°N-60°N), the Agulhas Current sector (10°E-90°E and 55°S-20°S), and the Southern Ocean sector (south of 35°S). Consistently with (6a), positive and negative values correspond to positive and negative trend of the mean temperature, respectively.

	Global	North Atlantic				Agulhas	Southern
10^{-11} K s^{-1}	Mean	All	West	Central	East	Current	Ocean
Total	3.9	6.8	34.4	0.3	-15.5	-12.5	-21.2

b. *Horizontal eddy-mean interactions*

Now that the overall mean and turbulent states have been described, we focus on the three interactions terms: total, non-local (or variance redistribution) and local (or variance transfers), following (7) and their horizontal expression (12). Our estimations suggest values of the order of a few 10^{-7} K^2 m^{-1} for the total and non-local term and of several 10^{-8} K^2 m^{-1} for the local term (Fig. 8). We find that 88% of the ocean is dominated by the non-local term over the local one ($\mathcal{A}|_{\mathrm{hor}}$ *vs* $\mathcal{T}|_{\mathrm{hor}}$). This is quite interesting as we know that on global scale the redistribution vanishes. This result is consistent with the one for momentum transfer (i.e., Kinetic Energy) where similar dominance was found (Sévellec et al., 2025a). Looking at the residual [i.e., $\mathcal{R}|_{\mathrm{hor}} - (\mathcal{A}|_{\mathrm{hor}} + \mathcal{T}|_{\mathrm{hor}})$] as a proxy for the diagnostic error of the eddy-mean interactions, we find that this term remains small, even compared to the local term (Fig. 8d).

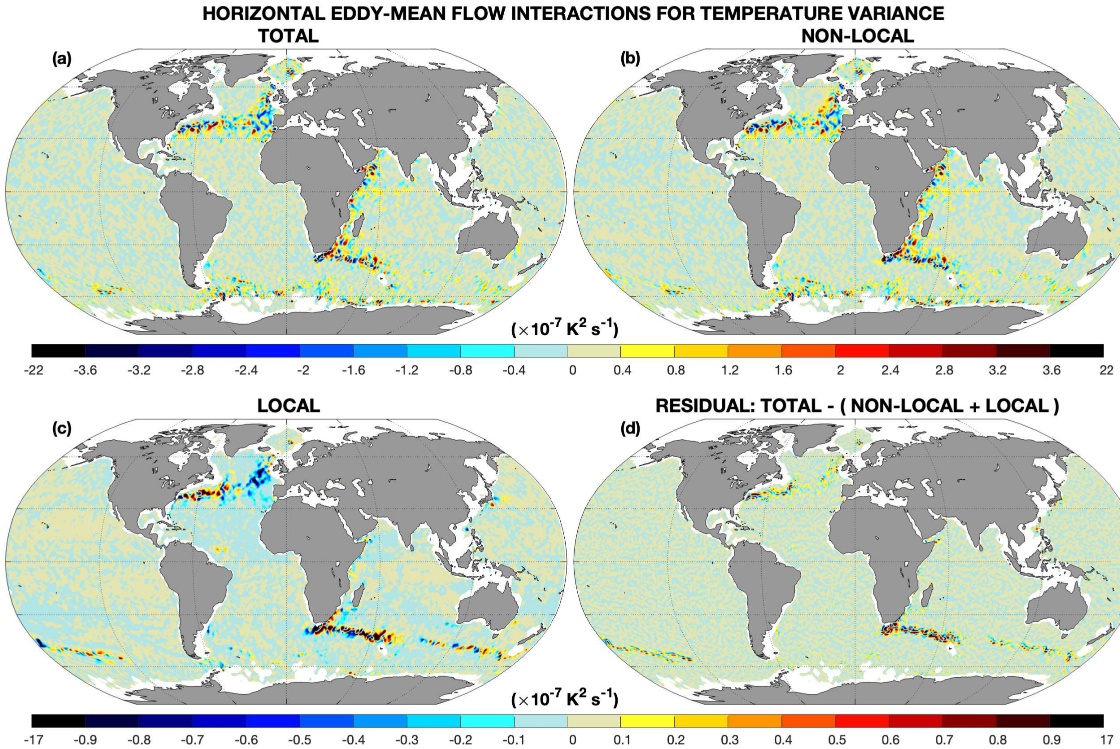

FIGURE 8: Components of the horizontal eddy-mean interactions for the temperature variance: (a) total ($\mathcal{R}|_{\mathrm{hor}}$), (b) non-local ($\mathcal{A}|_{\mathrm{hor}}$), (c) local ($\mathcal{T}|_{\mathrm{hor}}$), and (d) residual ($\mathcal{R}|_{\mathrm{hor}} - \mathcal{A}|_{\mathrm{hor}} - \mathcal{T}|_{\mathrm{hor}}$), following (12). The residual should be equal to 0 and so measures the estimation error of the eddy-mean interactions. Note the different colorscales for (a) and (b) *vs* (c) and (d). Positive and negative values correspond to variance transfers from ETV to MTV and from MTV to ETV, respectively.

The regions of strong interactions are mainly associated with regions of strong temperature variance rather than of strong eddy kinetic energy (Fig. 2). They correspond to the North Atlantic along the Gulf Stream and its associated North Atlantic Current, the Agulhas Current, and, but more moderately, the ACC (Fig. 8). The total and non-local terms have also a signature along the east coast of Africa and along the equator in the Indian Ocean (Fig. 8a and b). As expected from its expression ($\mathcal{T}|_{\rm hor}{=}2\,\overline{\boldsymbol{u}'_H T'}\big|_{\perp}\,\big\|\boldsymbol{\nabla}_H\bar{T}\big\|$) the local term is the projection of turbulent flux onto the mean temperature gradient (Fig. 8c *vs* Figs. 5 and 6b). Here the inconsistency between the observed turbulent flux and the downgradient closure becomes obvious and is potentially dramatic for temperature variance transfers. Indeed the existence of $\mathcal{T}|_{\rm hor}{>}0$ is directly related to the upgradient flux (regardless of the rotational term) and requires negative diffusivity coefficients for the Fick's law to be applied (Appendix). Hence at the $2^\circ{\times}2^\circ$-scale and for temperature variance budget, the observed variance transfers questions the validity of traditional downgradient flux turbulent closure (Redi, 1982) and the use and estimations of positive diffusivity coefficients (e.g., Klocker and Abernathey, 2014; Groeskamp et al., 2020; Roach et al., 2018; Sévellec et al., 2022).

Focusing on the two key regions: the North Atlantic and the Agulhas Current sector (as defined above), we see again that the non-local term is almost 4 times as large as the local one (Fig. 9). However patterns are more spatially-consistent for the local term than for the non-local term. Indeed the total and non-local terms show positive and negative values of typical spatial-scale of $\sim$5°, whereas the local term shows values which extend over almost $\sim$10°. In particular, in the eastern North Atlantic, the local term is almost exclusively negative, with the core of the pattern extending over $\sim$15° in both longitudes and latitudes. This suggests a region of intense variance transfers from the mean temperature to the turbulent one. We hypothesize that this region of (mostly) downgradient thermal turbulence is linked to "free" mesoscale turbulence (away from its formation in the Gulf Stream), consistent with (positive) trajectory dispersion (Taylor, 1921; Batchelor, 1949).

When globally-averaged the total interaction is negative with the expected dominance of the local term (Tab. 2). This suggests that variance is transferred from the mean to the turbulence. Looking at the 6 key regions (already defined above), the spatial-averages reveal that most regions are prone to negative interaction (i.e., destruction of the mean temperature structure) except for the west North Atlantic (Tab. 2). In this region the mean temperature structure is maintained whereas the temperature turbulence is decreased. In the west North Atlantic, Agulhas Current, and Southern Ocean the variance redistribution remains as intense as the variance transfer. This is consistent with region of intense current where advection plays a crucial role in redistributing variance. In all tested regions and globally the residual term is weak, suggesting the robustness of the computed diagnostics.

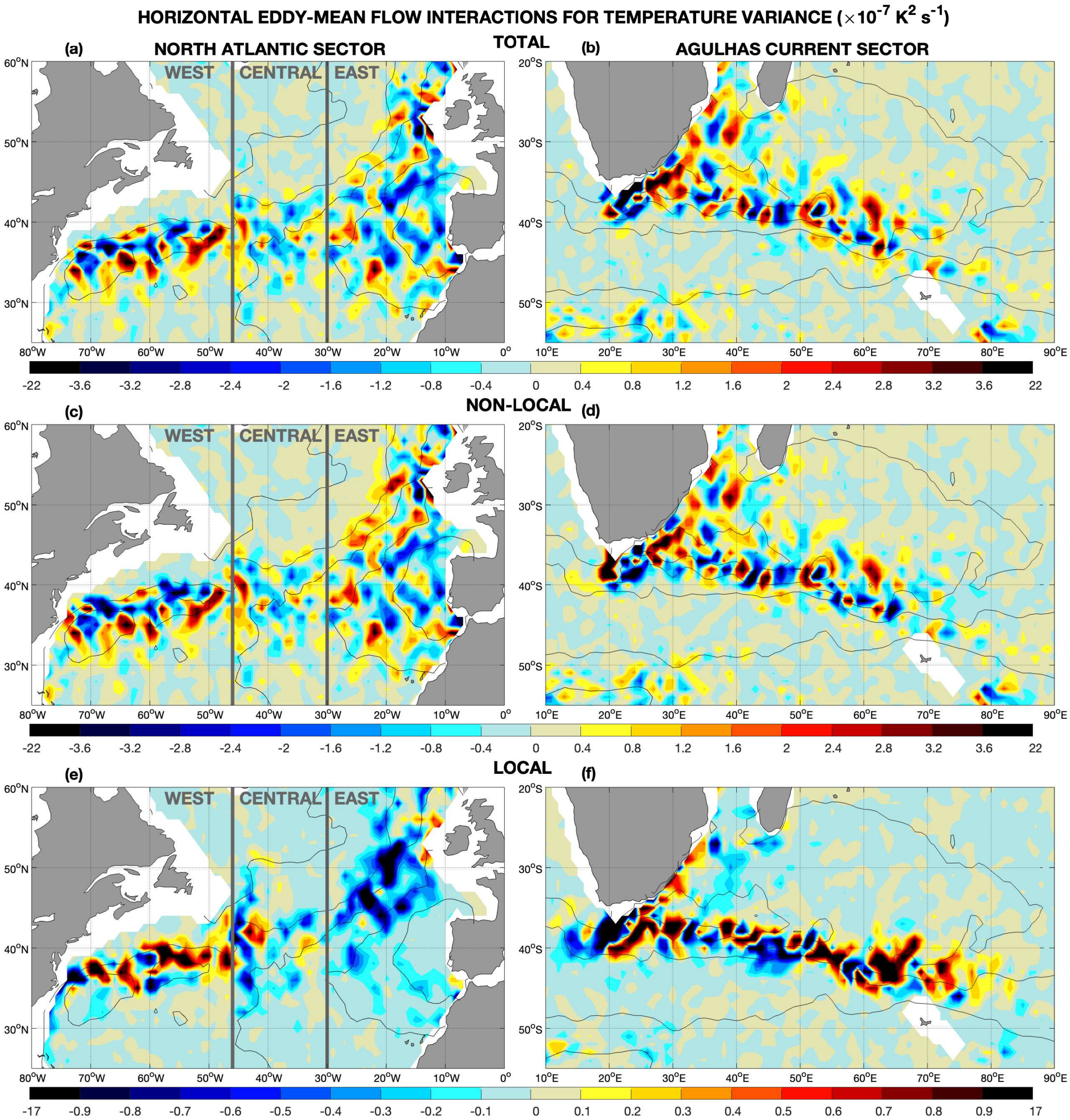

FIGURE 9: As Fig. 8 but zoomed for two key regions, (a, c, and e) the west and east North Atlantic sectors and (b, d, and f) the Agulhas Current sector. Components of the horizontal eddy-mean interactions for the temperature variance: (a-b) total ($\mathcal{R}|_{\text{hor}}$), (c-d) non-local ($\mathcal{A}|_{\text{hor}}$), and (e-f) local ($\mathcal{T}|_{\text{hor}}$), following (12). Positive and negative values correspond to variance transfers from ETV to MTV and from MTV to ETV, respectively. Contours show Conservative temperature with contours from $-2°$C to $13°$C with $1.5°$ contour interval.

Table 2: Spatial-averages of the horizontal variance transfers, following (12), both at global and regional level. The 6 regions (Fig. 9) corresponds to: the whole North Atlantic (80°W-0° and 25°N-60°N), the Western North Atlantic (80°W-46°W and 25°N-60°N), the Central North Atlantic (46°W-30°W and 25°N-60°N), the Eastern North Atlantic (30°W-0° and 25°N-60°N), the Agulhas Current sector (10°E-90°E and 55°S-20°S) and the Southern Ocean sector (south of 35°S). Positive and negative values correspond to variance transfers from ETV to MTV and from MTV to ETV, respectively. The residual reflects the error of the diagnostics.

	Global	North Atlantic				Agulhas	Southern
(10^{-9} K^2 s^{-1})	Mean	All	West	Central	East	Current	Ocean
Total	-0.5	-5.6	3.7	-5.5	-14.9	-0.4	-1.7
Non-Local	0.2	0.2	1.9	-0.2	-1.1	1.4	-0.8
Local	-0.7	-6.0	1.8	-5.2	-14.3	-1.5	-0.8
Residual	0.0	0.2	0.0	-0.1	0.5	-0.3	-0.1

c. *Consequences for mean-temperature distribution maintenance*

Since $\mathcal{T}$ is the only term that has a global impact and hence any impact on the width of the mean temperature distribution, we focus on this term in the following subsection.

We decompose the global variance transfer in term of temperature classes to determine how each class contributes to the overall shrinking of the mean temperature distribution. Following Water Mass transformations framework (Walin, 1982), one can derive the variance transformations as a function of temperature classes. This reads:

$$\Psi^{\#} = \rho_0 C_p \partial_{\bar{T}} \iint_{S\left(\bar{\Theta}'' \leq \bar{\Theta}\right)} \mathcal{T}\, ds \Delta z, \tag{17}$$

where $S\left(\bar{\Theta}'' \leq \bar{\Theta}\right)$ is ocean surface at 1 000 m with temperature lower than or equal to $\bar{\Theta}$, ρ_0 is the reference density, C_p is the ocean heat capacity, and Δz is an ocean layer thickness. As discussed in Sévellec et al. (2025b), Δz should be set based on the increment of the temperature classes to make $\Psi^{\#}$ independent of this increment choice. At this depth, Sévellec et al. (2025b) suggest the use of $\Delta z|_{\mathrm{ref}}$=70 m for a neutral density increment of $\Delta\gamma|_{\mathrm{ref}}$=0.03 kg m^{-3}. Hence, through a scaling, this corresponds to a thickness $\Delta z = \alpha \Delta T \Delta z|_{\mathrm{ref}} / \Delta\gamma|_{\mathrm{ref}}$=58.3 m for our temperature increment of ΔT=0.25 K (and a spatial-mean thermal expansion coefficient of α=0.1 kg m^{-3} K^{-1}).

This diagnostic reveals that for almost all the temperature classes the variance transfers contributes to the shrinking of mean temperature distribution (Fig. 10). This remarkable consistency contrasts with the intricate structure of the geographical distribution of the variance transfers (Fig. 8c). For a few water classes, however, the variance transfers lead to a broadening of the distribution. This is the case for extreme water classes: Conservative Temperature below 0.5°C and above 11.25°C. (Although this result has to be moderated since these temperature ranges correspond to poleward locations where there is the least amount of observations.) It is also the case for Conservative Temperature between 6.5°C and 7.25°C. Overall, the variance transformation is not proportional to the volume of water, for instance the AAIW has the largest volume, but this is not where the variance transformation maximum occurs. Basically the volume-distribution is sharper than the variance-transformations. Also there is a temperature-class lag of their distribution center with a peak at ∼4.5°C and between 5°C and 5.5°C for the former and the latter, respectively.

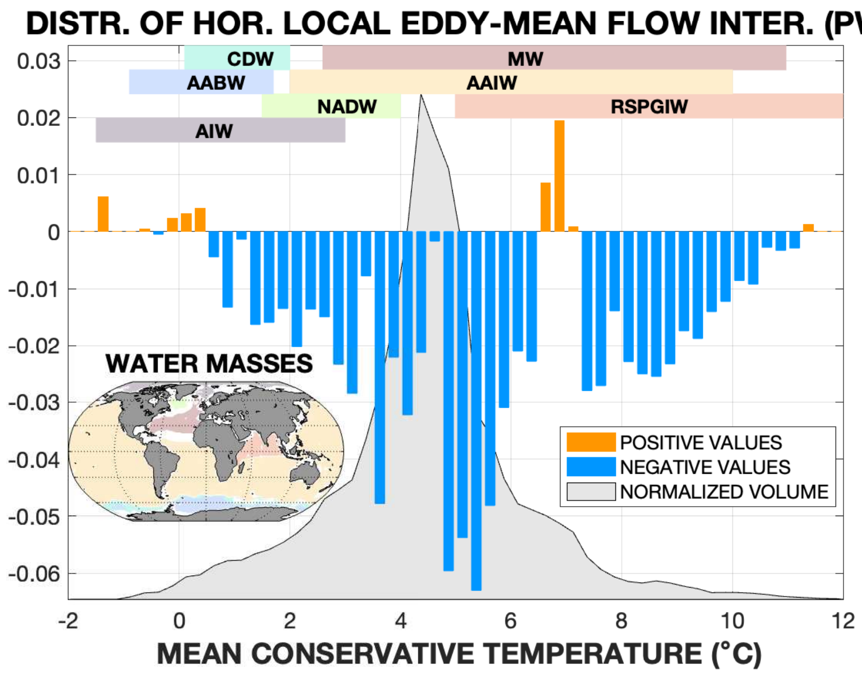

FIGURE 10: As Fig. 8c but as a distribution in terms of conservative temperature classes, following (17). This corresponds to the distribution of local eddy-mean interactions for the temperature variance ($\mathcal{T}|_{\text{hor}}$), following (12), as a function of the mean temperature. Positive (orange) and negative (cyan) values correspond to variance transfers from ETV to MTV and from MTV to ETV, respectively. The relative volume of each water class is given by the grey patch. Temperature classes are spaced by 0.25°C and the volume curves have been smoothed using a 1°C moving average. The horizontal color patches show properties of selected Water Masses: AntArctic Bottom Water (AABW), Circumpolar Deep Water (CDW), AntArctic Intermediate Water (AAIW), Red Sea–Persian Gulf Intermediate Intermediate Water (RSPGIW), Mediterranean Water (MW), North Atlantic Deep Water (NADW), and the Arctic Intermediate Water (AIW), following Emery (2018). These water mass locations are depicted in the inset.

To describe the variance transformations as a function of Water Masses, we first defined

7 main Water Masses located at 1 000-m depth. These correspond to the Arctic Intermediate Water (AIW: −1.50-3.00°C and 34.87-35.17 g kg^{-1}), the AntArctic Bottom Water (AABW: −0.90-1.70°C and 34.81-34.89 g kg^{-1}), the Circumpolar Deep Water (CDW: 0.10-2.00°C and 34.78-34.90 g kg^{-1}), the North Atlantic Deep Water (NADW: 1.50-4.00°C and 34.97-35.17 g kg^{-1}), the AntArctic Intermediate Water (AAIW: 2.01-10.00°C and 33.96-34.97 g kg^{-1}), the Mediterranean Water (MW: 2.60-10.97°C and 35.17-36.38 g kg^{-1}), and the Red Sea–Persian Gulf Intermediate Intermediate Water (RSPGIW: 5.00-13.98°C and 34.97-35.57 g kg^{-1}). The above Conservative Temperature and Absolute Salinity characteristics have been derived from Emery (2018) and positioned using both Conservative Temperature and Absolute Salinity from ISAS17 (inset of Fig. 10). This description allows for characterizing for water masses with a positive variance transformation: the CDW, the AABW, the RSPGIW and the mildest part of the MW (Fig. 10). On the other hand, the other Water Masses all correspond to an overall negative variance transfer of mean temperature variance. This sharpening of the temperature distribution is particularly active within the MW (Fig. 10).

d. Implications for mean-temperature structure balance

Moving back to the global-mean temperature variance transfers, at high Péclet number and at equilibrium ($\partial_t \bar{T}^2$=0), from (10) we have $2\left\langle \bar{T}\bar{F}\right\rangle = -\left\langle \mathcal{T}\right\rangle$. Assuming an optimal flux (i.e., perfect match with the temperature structure), we have $\bar{F}_{\text{opt}} = \phi\frac{\bar{T}}{\sigma_{\bar{T}}}$ (where ϕ is a scalar) and we obtain: $\phi = -\frac{1}{2}\frac{\langle\mathcal{T}\rangle}{\sigma_{\bar{T}}}$. Applying it to our horizontal framework, the minimum heat flux amplitude to balance the transfer terms is $\phi|_{\text{hor}}$=2.0×10^{-10} K s^{-1} or 4.7×10^{-2} W m^{-2} (after multiplying by $\rho_o C_p \Delta z$ to obtain an equivalent heat flux). This suggests that the minimal heat flux to maintain the horizontal temperature structure at 1 000 m given the action of the turbulence corresponds to a warming of ∼1 K per 150 years.

Since this study focuses only on the horizontal component, the reference conservative temperature is a horizontal average (i.e., $\langle\Theta\rangle_{\text{hor}}$). Hence a pseudo-vertical advection of the form $\bar{w}\partial_z\left\langle\Theta\right\rangle_{\text{hor}}$ was incorporated to the mean-temperature evolution equation as a forcing term, as explained in section 3a.. At 1 000-m depth, this should be the main/key term in the forcing term (i.e., $\bar{F}\big|_{\text{hor}}$). This allows for the computation of an optimal vertical velocity, following $\bar{F}_{\text{opt}}\big|_{\text{hor}} = -\bar{w}_{\text{opt}}\partial_z\left\langle\Theta\right\rangle_{\text{hor}}$ and using the expression of $\bar{F}_{\text{opt}}$ provided above. This reads:

$$\bar{w}_{\text{opt}} = \frac{\bar{T}}{2\partial_z\left\langle\Theta\right\rangle_{\text{hor}}}\frac{\left\langle\mathcal{T}|_{\text{hor}}\right\rangle_{\text{hor}}}{\sigma^2_{\bar{T}}\big|_{\text{hor}}}, \tag{18}$$

where $\sigma^2_{\bar{T}}\big|_{\text{hor}}$=$\langle\bar{T}^2\rangle_{\text{hor}}$ is the horizontal variance of the mean temperature. This corresponds to a transfer from the reference state ($\langle\Theta\rangle_{\text{hor}}$) to the mean temperature structure ($\bar{T}^2$) by mean vertical motions ($\bar{w}$). This is equivalent to a transfer between the Background Potential

Energy and the Available Potential Energy, in the context of potential energy transfers. (Note that, even at equilibrium, the equality linking variance transfers and forcing is only true on global average, since locally advection can transport from local sources to local sinks.) Since the ANDRO database does not contain observations of vertical temperature shear, we computed it from the ISAS product (Kolodziejczyk et al., 2023). We find values of $\bar{w}_{\mathrm{opt}}$ of the order of 10^{-7} m s^{-1} (Fig. 11), which corresponds to about a centimeter per day. This values is weaker and so consistent with mesoscale vertical velocity estimations of Christensen et al. (2004). As expected from the formulation of (18), the horizontal structure varies together with the mean temperature. This leads to upwelling of the colder waters: AABW, CDW, NADW, and AIW; and downwelling of MW and RSPGIW (as well as of its residual within the recirculation of the Agulhas Current); the AAIW is both upwelled and downwelled depending if it is below or above a conservative temperature of $\langle\Theta\rangle_{\mathrm{hor}}\simeq 4.36°$C (this threshold is an obvious consequence of the definition of $T=\Theta-\langle\Theta\rangle_{\mathrm{hor}}$). Maximum upwelling occurs in the Nordic Seas, whereas downwelling occurs off the Portugal coast.

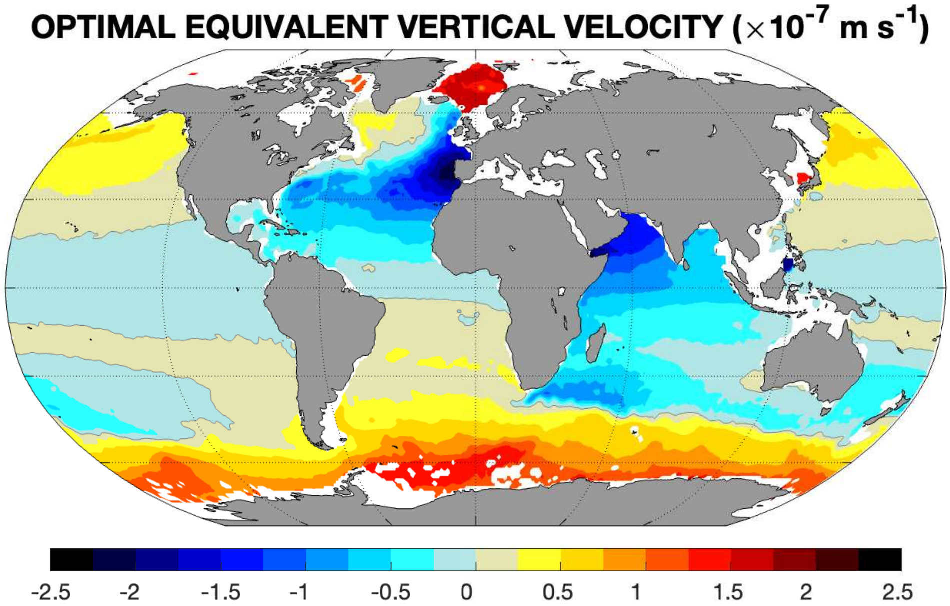

FIGURE 11: Optimal equivalent vertical velocity, following (18). This vertical velocity leads to the most efficient mean vertical advection allowing for a global compensation of the variance transfer ($\mathcal{T}$). (Note that, even at equilibrium, there is no need for a perfect local compensation, since advection can transport variance from local sources to local sinks.) Grey contour shows Conservative Temperature of $\langle\Theta\rangle_{\mathrm{hor}}\simeq 4.36°$C and perfectly matches $\bar{w}_{\mathrm{opt}}=0$ by construction of the anomalous Conservative Temperature (i.e., $T=\Theta-\langle\Theta\rangle_{\mathrm{hor}}$).

Comparison with actual vertical velocity at 1 000-m depth (w_{real}) should be done carefully.

Indeed the optimal vertical velocity is the minimum vertical velocity needed to balance the temperature variance transfers, so it does not have to exactly reflect the real velocity. Hence, the actual vertical velocity only needs to contain the optimal velocity for consistency. Liang et al. (2017) and Cortés-Morales and Lazar (2024) have provided estimations of the vertical velocity, and in particular at 1 000-m depth. It corresponds to a flow of a few to several 10^{-6} m s^{-1}. This is, at least, one order of magnitude above the required optimal velocity. At this depth the retrieved estimated vertical velocity pattern bears a resemblance to the Ekman (1905) pumping pattern (Marshall and Plumb, 2007; Wunsch, 2011; Roquet et al., 2011). Hence w_{real} corresponds to upwelling in the subpolar regions and a downwelling in the poleward part of subtropical regions (north of 30°N and south of 30°S for the northern and southern hemisphere, respectively). This is overall quite consistent with our optimal vertical velocity (Fig. 11). In particular, positive values in the subpolar North Atltantic and North Pacific, positive values in Southern Ocean, negative values along the North Atlantic Current and within the Mediterranean Water, and negative values within the Agulhas current, its retroflection, and its merging with the ACC are all consistent signatures of both w_{real} and w_{opt}. This suggests the positive projection of w_{opt} onto w_{real} and that w_{opt} can be indeed contained within w_{real}. Hence, even if not a perfect validation of w_{opt}, we can conclude that independent estimations of w_{real} are consistent with our framework and results. This suggests that the observed mean upwelling has the potential to balance the variance transfers estimated in the present study.

5 Discussions

In this study, we have developed a consistent framework to track and assess the eddy-mean interactions of temperature variance. To this purpose we have built on analyses of variance budget (e.g., Sévellec et al., 2006; Buckley et al., 2012; Sévellec et al., 2021) and of Kinetic Energy interactions (e.g., Chen et al., 2014, 2016; Sévellec et al., 2025a) to disentangle the temperature variance exchanges between the mean and the turbulence. This framework has some analogy with studies looking at potential energy exchanges (e.g., Kang and Curchitser, 2015; Chen et al., 2016; Jamet et al., 2024). We find that the eddy-mean interactions are well described using three reservoirs: the Mean Temperature Variance, the Residual Temperature Variance, and the Eddy Temperature Variance (Fig. 3). They correspond to the zeroth, first, and second order terms of the temperature square, respectively. The RTV is peculiar in the sense that it is zero on average, but it is key in the sense that it acts as a mediator between MTV and ETV. In this context, we have shown that the total interactions are the sum of the non-local and local interactions, where the former corresponds to a temperature variance redistribution and the latter corresponds to the temperature variance transfers.

To compute the temperature variance interactions we have used consistent, *in situ* global observations of temperature and horizontal velocity provided by the ANDRO dataset (Ollitrault and Rannou, 2013). The ANDRO dataset is based on deep Argo float displacements, limiting our study to 1 000-m depth. We find that the across-isothermal turbulent temperature fluxes are only 55% downgradient, challenging the applicability of downgradient flux closure (Redi, 1982) to accurately represent temperature variance transfers. Regarding the temperature variance interactions, the pattern shows intensification in the Gulf Stream, in the North Atlantic Current, in the Agulhas retroflection, and in both ACC of the Indian Ocean sector and of the Pacific Ocean sector. The typical length scale signature varies from several degrees to around a dozen of degrees. At the scale of the computation (i.e., $2°\times2°$), the non-local terms are more intense than the local terms, leading to their dominance on the total interactions.

When averaged over larger area, in almost all tested regions and in the global average the variance transfers (i.e., local term – $\mathcal{T}$) is negative and is the dominant term for the eddy-mean interactions (i.e., total term – $\mathcal{R}$). This suggests a shrinking of the mean temperature distribution (restoring toward the mean value, consistently with the intuitive description of Zika et al., 2012) and an intensification of turbulent activity. This view is also correct when looking at average effect over mean temperature classes, where most of them correspond to a shrinking of the mean temperature distribution. This suggests that, unlike for the $2°\times2°$-scale, the downgradient flux closure can represent accurately water mass variance transformation. In contrast, the western North Atlantic is the only tested region where the turbulence acts to broaden the mean temperature distribution, whereas turbulent activity is damped. Hence this region acts as a graveyard for turbulence allowing the maintenance of mean-temperature structure, hence of the mean-circulation. Extrapolating this result to the full water column, this is consistent with this particular region being a warm region ($\bar{T}>0$) where the ocean releases heat to the atmosphere ($\bar{F}< 0$, Tomita et al., 2021, for instance), and so having a negative correlation between heat flux and anomalous temperature field ($\bar{T}\bar{F}<0$). This leads to a mean temperature damping effect by the heat flux ($\partial_t\bar{T}^2<0$), which needs to be maintained by turbulence processes ($\mathcal{T}>0$). This is also supported by the relatively important positive contribution of the variance redistribution (i.e., nonlocal term – $\mathcal{A}$) which also compensates the action of the heat flux and contributes to the maintenance the mean temperature structure of this region.

Even if our study is only centered around the 1 000-m depth, the properties of the interactions give us a unique observational insight on the dynamics of the ocean. Indeed, generalizing our results that the global-mean variance transfers are negative ($\langle\mathcal{T}\rangle<0$) has implication for the ocean equilibrium. To this purpose we first need to acknowledge a few properties: the large-scale dissipation term is negligible (i.e., high Péclet number: $\langle\bar{T}\bar{D}\rangle\simeq0$), the small-scale dissipation is of leading order and negative (as demonstrated in this study:

$\langle\overline{T'D'}\rangle\leq 0$), the large-scale forcing is positive (i.e., warming in warm areas and cooling in cold areas: $\langle\bar{T}\bar{F}\rangle > 0$), and we can hypothesize that the small-scale forcing, if it exists, is negative (i.e., warm and cold eddies transfer their properties to the atmosphere: $\langle\overline{T'F'}\rangle\leq 0$). This leads to the conclusion that, at equilibrium and globally, the mean large-scale forcing is either re-injected to the atmosphere as small-scale forcing or is transferred toward turbulent small-scale ocean dissipation: $\xrightarrow{2\langle\bar{T}\bar{F}\rangle}\sigma^2_{\bar{T}}\xrightarrow{\mathcal{T}}\langle\sigma^2_{T'}\rangle\underset{2\langle\overline{T'D'}\rangle}{\xrightarrow{2\langle\overline{T'F'}\rangle}}$. This is a (partial) observational evidence of the direct cascade of temperature variance, already established in an idealized-configuration modeling study (Hochet et al., 2020), similar to the expected direct cascade of potential energy (Rhines, 1977; Salmon, 1978, 1980). This means that the large-scale forcing broadens the large-scale distribution which is balanced by a shrinking effect of variance transfers toward small-scale variance, this small-scale variance increases being balanced by small-scale dissipation or possibly a net anti-correlation of small-scale forcing and small-scale temperature anomaly. Hence our study opens the possibility of rationalizing the ocean as a "device" converting large-scale forcing from the atmosphere to small-scale forcing to the atmosphere (Small et al., 2008) with some efficiency (i.e., small-scale ocean dissipation). Determining the relative effect of small-scale forcing and small-scale dissipation will be the goal of future analyses.

One consequence of our framework consistently with our limited dataset (i.e., a single slice of the ocean at 1 000-m depth) is the need to define a background mean temperature gradient ($\partial_z \langle\Theta\rangle$). This background provides a source of variance through vertical motion impacting the mean temperature variance. This has allowed us to estimate an optimal vertical velocity needed to compensate the transfers toward the eddy variance, which corresponds to only a few centimeter per day. Whereas the Abyssal Recipes allows for an estimation of the required turbulence based on observed circulation (Munk and Wunsch, 1998), here we have used turbulence observations to estimate the required vertical velocity. This background ($\langle\Theta\rangle_{\mathrm{hor}}$) bears obvious resemblance with the reference state used to define the Background Potential Energy (Lorenz, 1955; Hochet et al., 2022), whereas the MTV and ETV ($\bar{T}^2$ and T'^2) are analog to the mean- and eddy- Available Potential Energy (Lorenz, 1955; Hochet et al., 2022), respectively. Building on this relation might help define the background temperature, central to our study, in a robust, physically-meaningful, and elegant manner.

Our study being at a single depth, it obviously suffers from a limited view. Building a full three-dimensional picture based on observations of the eddy-mean interactions of temperature, salinity, and density variance will be the goal of future investigations. Beyond observations, testing our framework and results in long climate simulations which include eddy-resolving ocean models is a direction for future work. Indeed our study provides an observational estimate that can help test and validate eddy-resolving ocean numerical simulations. It also provides a step forward for further developments and implementations of ocean turbulent closures for laminar ocean numerical models.

Appendix: physical interpretation of the eddy-mean interactions

In this appendix, we derived the turbulent heat flux as well as the total, local, and non-local interactions following two classical frameworks. This provides physical interpretations of the eddy-mean interaction terms.

Rotationial and divergent decomposition

Following the Helmholtz decomposition, Marshall and Shutts (1981) and Fox-Kemper et al. (2003) suggested that the turbulent heat flux can be decomposed into a divergent and a rotational component. This reads:

$$\overline{\boldsymbol{u}'T'}\big|_{\mathrm{div}} = \boldsymbol{\nabla}\phi, \tag{A1a}$$

$$\overline{\boldsymbol{u}'T'}\big|_{\mathrm{rot}} = \boldsymbol{\nabla}\times\boldsymbol{A}, \tag{A1b}$$

where ϕ is a scalar potential and $\boldsymbol{A}$ is a vector potential. (Note that ϕ and $\boldsymbol{A}$ are not uniquely defined, Fox-Kemper et al., 2003, leading, in practice, to the indeterminacy decomposition.) This framework leads a simplification of the flux divergence acting on the mean-temperature, as indicated in (6a):

$$\boldsymbol{\nabla}^{\dagger}\cdot\overline{\boldsymbol{u}'T'}\big|_{\mathrm{div}} = \nabla^2\phi, \tag{A2a}$$

$$\boldsymbol{\nabla}^{\dagger}\cdot\overline{\boldsymbol{u}'T'}\big|_{\mathrm{rot}} = 0, \tag{A2b}$$

where ∇^2 is the Laplacian ($=\boldsymbol{\nabla}^{\dagger}\cdot\boldsymbol{\nabla}=\partial_x^2+\partial_y^2+\partial_z^2$). This implies that only the divergent term is important for the mean-temperature evolution (Marshall and Shutts, 1981). (A2) is now routinely applied in oceanographic studies (e.g., Aoki et al., 2013; Guo and Bishop, 2022). It potentially solves the apparent paradox of the important (45%) upgradient turbulent heat fluxes: part of them can come from the rotational term.

For the variance transfers [i.e., local interactions: $\mathcal{T}=2\left(\boldsymbol{\nabla}\bar{T}\right)^{\dagger}\cdot\overline{\boldsymbol{u}'T'}$], both divergent and rotational components are potentially important. However we have:

$$\left(\boldsymbol{\nabla}\bar{T}\right)^{\dagger}\cdot\overline{\boldsymbol{u}'T'}\big|_{\mathrm{rot}} = \boldsymbol{\nabla}^{\dagger}\cdot\left(\bar{T}\,\overline{\boldsymbol{u}'T'}\big|_{\mathrm{rot}}\right). \tag{A3}$$

Hence, assuming no net variance flux at the boundaries, we know that:

$$\iiint_V \left(\boldsymbol{\nabla}\bar{T}\right)^{\dagger}\cdot\overline{\boldsymbol{u}'T'}\big|_{\mathrm{rot}}\,dv = 0. \tag{A4}$$

This means that the rotational component does not contribute to a net global temperature variance transfer.

We can conclude that, at the computational scale, both divergent and rotational components will be at play for the transfers and that the upgradient and downgradient properties of the turbulent heat flux select the direction of the transfers (i.e., toward the mean and toward the eddy, respectively). However at global-scale only the divergent component contributes. We hypothesize that there exists a spatial-scale over which the rotational component of the transfers vanishes. Under this assumption, a downgradient closure of the divergent component is consistent with our observations of negative transfers at global-scale and for most tested spatial and Water Mass averages (Tab. 2 and Fig.10). Whereas this downgradient closure would be valid at all-scale for the mean-temperature evolution, it would only be valid over this hypothesized spatial-scale for variance transfers.

Symmetric and antisymmetric decomposition

Here we follow an other classical theoretical framework, namely the Temporal-Residual-Mean (McDougall and McIntosh, 2001). This framework shows that the turbulent temperature flux can be represented through the mean temperature gradient. This reads:

$$\overline{\boldsymbol{u}'T'} \sim -\left(\mathbf{A} + \mathbf{S}\right) \cdot \boldsymbol{\nabla}\bar{T}, \tag{A5}$$

where $\mathbf{A}$ and $\mathbf{S}$ are antisymmetric and symmetric tensors, respectively. They represent rotation and deformation associated to eddy advection and diffusion closure, respectively.

Applying it to the total, local, and non-local interaction terms, following (7), we have:

$$\mathcal{R} = -2\bar{T}\boldsymbol{\nabla}^{\dagger} \cdot \overline{\boldsymbol{u}'T'} \sim \boldsymbol{\nabla}^{\dagger} \cdot \left[\left(\mathbf{A} + \mathbf{S}\right) \cdot \boldsymbol{\nabla}\bar{T}^{2}\right] - 2\left(\boldsymbol{\nabla}\bar{T}\right)^{\dagger} \cdot \mathbf{S} \cdot \boldsymbol{\nabla}\bar{T}, \tag{A6a}$$

$$\mathcal{A} = -2\boldsymbol{\nabla}^{\dagger} \cdot \left(\bar{T}\overline{\boldsymbol{u}'T'}\right) \sim \boldsymbol{\nabla}^{\dagger} \cdot \left[\left(\mathbf{A} + \mathbf{S}\right) \cdot \boldsymbol{\nabla}\bar{T}^{2}\right], \tag{A6b}$$

$$\mathcal{T} = 2\left(\boldsymbol{\nabla}\bar{T}\right)^{\dagger} \cdot \overline{\boldsymbol{u}'T'} \sim -2\left(\boldsymbol{\nabla}\bar{T}\right)^{\dagger} \cdot \mathbf{S} \cdot \boldsymbol{\nabla}\bar{T}, \tag{A6c}$$

These formulation help us reinterpret the local and non-local terms. The non-local term corresponds to the eddy-advection and eddy-diffusion of mean temperature variance (exhibiting the action of both antisymmetric and symmetric tensor). They correspond to a spatial-redistribution of variance (i.e., conserving the global mean-variance). With this formulation, the residual temperature variance appears less useful as the mean temperature variance is self-consistent (as expected for the Temporal-Residual-Mean framework, McDougall and McIntosh, 2001). At the opposite, the local term is only controlled by the symmetric tensor. Also its global integral does not vanish. This implies the possibility of a net global variance transfer between mean and eddy temperature variance. Consequently and as mentioned in McDougall and McIntosh (2001) for density, only the symmetric component acts on the eddy temperature variance.

To further characterize the physical constraint behind the local term, we can split the symmetric tensor through an eigen-decomposition. The local term becomes:

$$\left(\boldsymbol{\nabla}\bar{T}\right)^{\dagger} \cdot \mathbf{S} \cdot \boldsymbol{\nabla}\bar{T} = \sum_{i=1}^{3} \kappa_i \left(\boldsymbol{s}_i^{\dagger} \cdot \boldsymbol{\nabla}\bar{T}\right)^2, \tag{A7}$$

where κ_i are the three diffusivity coefficients along the three natural direction $\boldsymbol{s}_i$, such as $\mathbf{S}=\sum_{i=1}^{3} \kappa_i \boldsymbol{s}_i \cdot \boldsymbol{s}_i^{\dagger}$ (i.e., an eigen-decomposition of $\mathbf{S}$). Hence $\mathcal{T}>0$ can only come from a negative diffusivity coefficient (κ_i), reminiscent of the negative viscosity of Starr (1968).

This formulation suggests that, beyond the existence of rotational fluxes, the existence of $\mathcal{T}>0$ (Fig. 8c) is inconsistent with the Fick's law closure. Only when averaged over large spatial-scale or water masses this downgradient flux closure appears consistent with our observations (Tab. 2 and Fig. 10, respectively), except for a few peculiar regions or water classes. It is worth noting that state-of-the-art direct and indirect estimations often lead, sometimes by construction, to positive definite diffusivity coefficients (e.g., Klocker and Abernathey, 2014; Groeskamp et al., 2020; Roach et al., 2018; Sévellec et al., 2022). This has the inherent consequence of restricting variance transfers from the mean to the eddy.

Acknowledgment. This work was supported by ARVOR, OASIS, and VACARM projects from LEFE IMAGO and GMMC programs, and by the OceaniX project funded through the French ANR program, and by the ISblue project, Interdisciplinary graduate school for the blue planet (ANR-17-EURE-0015) co-funded by a grant from the French government under the program "Investissements d'Avenir". ANDRO Argo floats displacements product is made freely available by SNO Argo France at LOPS Laboratory (supported by UBO/CNRS/Ifremer/IRD) and IUEM Observatory (OSU IUEM/CNRS/INSU), and was funded by Ifremer, Coriolis, SOERE-CTDO2, SNO Argo France, and CPER region Bretagne OBSOCEAN. Florian Sévellec, Antoine Hochet, and Thierry Huck are supported by the EERIE project (Grant Agreement No 101081383) funded by the European Union. Views and opinions expressed are however those of the authors only and do not necessarily reflect those of the European Union or the European Climate Infrastructure and Environment Executive Agency (CINEA). Neither the European Union nor the granting authority can be held responsible for them.

Data Availability. The ANDRO dataset used in this study corresponds to the 2025 Release (key: '116520') and is available at `https://doi.org/10.17882/47077`. The ISAS17 dataset provides a global three-dimensional gridded temperature and salinity data derived from objective analysis of in situ observations and is available at https://doi.org/10.17882/52367.

References

Aoki, K., S. Minobe, Y. Tanimoto, and Y. Sasai, 2013: Southward eddy heat transport occurring along southern flanks of the kuroshio extension and the gulf stream in a 1/108 global ocean general circulation model. *J. Phys. Oceanogr.*, **43**, 1899–1910.

Arzel, O., T. Huck, and A. Colin de Verdière, 2006: The different nature of the interdecadal variability of the thermohaline circulation under mixed and flux boundary conditions. *J. Phys. Oceanogr.*, **36**, 1703–1718.

Batchelor, G. K., 1949: Diffusion in a field of homogeneous turbulence. *Australian Journal of Scientific Research*, **2**, 437–450.

Bretherton, F. P., R. Davis, and C. Fandry, 1976: Technique for objective analysis and design of oceanographic experiment applied to MODE-73. *Deep-Sea Res. Oceanogr. Abstr.*, **23**, 559–582.

Buckley, M. W., D. Ferreira, J.-M. Campin, J. Marshall, and R. Tulloch, 2012: On the relationship between decadal buoyancy anomalies and variability of the atlantic meridional overturning circulation. *J. Climate*, **25**, 8009–8030.

Charney, J., 1947: The dynamics of long waves in a baroclinic westerly current. *J. Meteor.*, **4**, 135–162.

Chelton, D. B., M. G. Schlax, S. R. M. and R. A. deSzoeke, 2007: Global observations of large oceanic eddies. *Geophys. Res. Lett.*, **34**, L15 606.

Chen, R., G. R. Flierl, and C. Wunsch, 2014: A description of local and nonlocal eddy-mean flow interaction in a global eddy-permitting state estimate. *J. Phys. Oceanogr.*, **44**, 2336–2352.

Chen, R., A. F. Thompson, and G. R. Flierl, 2016: Time-dependent eddy-mean energy diagrams and their application to the ocean. *J. Phys. Oceanogr.*, **46**, 2827–2850.

Christensen, K., A. R. Gray, and S. C. Riser, 2004: Global estimates of mesoscale vertical velocity near 1,000 m from argo observations. *J. Geophys. Res.: Oceans*, **129**, e2023JC020 003.

Colin de Verdière, A., and R. Tailleux, 2005: The interaction of a baroclinic mean flow with long rossby waves. *J. Phys. Oceanogr.*, **35**, 865–879.

Cortés-Morales, D., and A. Lazar, 2024: Vertical velocity 3D estimates from the linear vorticity balance in the North Atlantic ocean. *J. Phys. Oceanogr.*, **54**, 2185–2203.

Eady, E. T., 1949: Long waves and cyclone waves. *Tellus*, **1**, 33–52.

Ekman, V. W., 1905: On the influence of the earth's rotation on ocean currents. *Ark. Mat. Astron. Fys.*, **2**, 1–52.

Emery, W. J., 2018: Ocean circulation — Water Types and Water Masses. *Encyclopedia of Atmospheric Sciences*, J. R. Holton, Ed., Academic Press, Oxford, 1556–1567.

Eyring, V., S. Bony, G. A. Meehl, C. A. Senior, B. Stevens, R. J. Stouffer, and K. E. Taylor, 2016: Overview of the coupled model intercomparison project phase 6 (CMIP6) experimental design and organization. *Geosci. Model Dev.*, **9**, 1937–1958.

Ferrari, R., and C. Wunsch, 2009: Ocean circulation Kinetic Energy: Reservoirs, sources, and sinks. *Annu. Rev. Fluid Mech.*, **41**, 253–282.

Fox-Kemper, B., R. Ferrari, and J. Pedlosky, 2003: On the indeterminacy of rotational and divergent eddy fluxes. *J. Phys. Oceanogr.*, **33**, 478–483.

Gaillard, F., T. Reynaud, V. Thierry, N. Kolodziejczyk, and K. von Schuckmann, 2016: In-situ based reanalysis of the global ocean temperature and salinity with ISAS: variability of the heat content and steric height. *J. Climate*, **29**, 1305–1323.

Groeskamp, S., J. H. LaCasce, T. J. McDougall, and M. Rogé, 2020: Full-depth global estimates of ocean mesoscale eddy mixing from observations and theory. *Geophys. Res. Lett.*, **47**, e2020GL089 425.

Guo, Y., and S. P. Bishop, 2022: Surface divergent eddy heat fluxes and their impacts on mixed layer eddy-mean flow interaction. *J. Adv. Model. Earth Syst.*, **14**, 805–807.

Hochet, A., T. Huck, O. Arzel, F. Sévellec, and A. Colin de Verdière, 2022: Energy transfers between multidecadal and turbulent variability. *J. Climate*, **35**, 1157–1178.

Hochet, A., T. Huck, O. Arzel, F. Sévellec, M. Mazloff, B. Cornuelle, and A. Colin de Verdière, 2020: Direct temporal cascade of temperature variance in eddy-permitting simulations of multidecadal variability. *J. Climate*, **33**, 9409–9425.

Hochet, A., C. Lique, F. Sévellec, and W. Llovel, 2024a: Drivers of interannual salinity variability in the arctic ocean. *J. Geophys. Res.: Oceans*, **29**, e2023JC020 852.

Hochet, A., W. Llovel, T. Huck, and F. Sévellec, 2024b: Advection-surface flux balance controls the seasonal steric sea level amplitude. *Sci. Rep.*, **14**, 10 644.

Hochet, A., W. Llovel, F. Sévellec, and T. Huck, 2023: Sources and sinks of interannual steric sea level variability. *J. Geophys. Res.: Oceans*, **128**, e2022JC019 335.

Holland, W. R., 1978: The role of mesoscale eddies in the general circulation of the ocean–numerical experiments using a wind-driven quasi-geostrophic model. *J. Phys. Oceanogr.*, **8**, 363–392.

Jamet, Q., A. Berger, B. Deremble, and T. Penduff, 2024: Thermodynamical effects of ocean current feedback in a quasigeostrophic coupled model. *J. Phys. Oceanogr.*, **54**, 1691–1704.

Jamet, Q., S. Leroux, W. K. Dewar, T. Penduff, J. Le Sommer, J.-M. Molines, and J. Gula, 2022: Non-local eddy-mean kinetic energy transfers in submesoscale-permitting ensemble simulations. *J. Adv. Model. Earth Syst.*, **14**, e2022MS003 057.

Kang, D., and E. N. Curchitser, 2015: Energetics of eddy-mean flow interactions in the Gulf Stream region. *J. Phys. Oceanogr.*, **45**, 1103–1120.

Klocker, A., and R. Abernathey, 2014: Global patterns of mesoscale eddy properties and diffusivities. *J. Phys. Oceanogr.*, **44**, 1030–1046.

Kolodziejczyk, N., A. Prigent-Mazella, and F. Gaillard, 2023: ISAS temperature, salinity, dissolved oxygen gridded fields. *SEANOE*, https://doi.org/10.17882/52367.

Liang, X., M. Spall, and C. Wunsch, 2017: Global ocean vertical velocity from a dynamically consistent ocean state estimate. *J. Geophys. Res.: Oceans*, **122**, https://doi.org/10.1002/2017JC012 985.

Lorenz, E. N., 1955: Available Potential Energy and the maintenance of the general circulation. *Tellus*, **VII**, 2, 157–167.

Marshall, J., and R. A. Plumb, 2007: *Atmosphere, Ocean and Climate Dynamics: An Introductory Text*. Academic Press, 344pp pp.

Marshall, J., and G. Shutts, 1981: A note on rotational and divergent eddy fluxes. *J. Phys. Oceanogr.*, **11**, 1677–1680.

Matsuta, T., and Y. Masumoto, 2021: Modified view of energy budget diagram and its application to the Kuroshio extension region. *J. Phys. Oceanogr.*, **51**, 1163–1175.

McDougall, T. J., and P. M. Barker, 2011: Getting started with teos-10 and the gibbs seawater (gsw) oceanographic toolbox. Tech. rep., SCOR/IAPSO WG127, 28pp pp.

McDougall, T. J., S. Groeskamp, and S. M. Griffies, 2014: On geometrical aspects of interior ocean mixing. *J. Phys. Oceanogr.*, **44**, 2164–2175.

McDougall, T. J., and P. C. McIntosh, 2001: The Temporal-Residual-Mean velocity. part II: Isopycnal interpretation and the tracer and momentum equations. *J. Phys. Oceanogr.*, **31**, 1222–1246.

Munk, W., and C. Wunsch, 1998: Abyssal recipes II : Energetics of tidal and wind mixing. *Deep-Sea Res. Part I*, **45**, 1977–2010.

Murakami, S., 2011: Atmospheric local energetics and energy interactions between mean and eddy fields. Part I: Theory. *J. Atmos. Sci.*, **68**, 760–768.

Murakami, S., R. Ohgaito, and A. Abe-Ouchi, 2011: Atmospheric local energetics and energy interactions between mean and eddy fields. Part II: An example for the last glacial maximum climate. *J. Atmos. Sci.*, **68**, 533–552.

Ollitrault, M., and J. P. Rannou, 2013: An Argo-based deep displacement datase. *J. Atmos. Oceanic Technol.*, **30**, 759–788.

Ollitrault, M., P. Rannou, E. Brion, C. Cabanes, A. Piron, G. Reverdin, and N. Kolodziejczyk, 2025: ANDRO: An Argo-based deep displacement dataset. *SEANOE*, https://doi.org/10.17882/47077.

Redi, M. H., 1982: Oceanic isopycnal mixing by coordinate rotation. *J. Phys. Oceanogr.*, **12**, 1154–1158.

Rhines, P. B., 1977: The dynamics of unsteady currents. *The Sea*, **Vol. VI**, John Wiley and Sons, New York.

Rhines, P. B., and W. R. Holland, 1979: A theoretical discussion of eddy-driven mean flows. *Dyn. Atmos. and Oceans*, **3**, 289–325.

Roach, C. J., D. Bawada, and K. Speer, 2018: Global observations of horizontal mixing from Argo float and surface drifter trajectories. *J. Geophys. Res.: Oceans*, **123**, doi:10.1029/2018JC013 750.

Roquet, F., C. Wunsch, and G. Madec, 2011: On the patterns of wind-power input to the ocean circulation. *J. Phys. Oceanogr.*, **41**, 2328–2342.

Salmon, R. B., 1978: Two-layer quasi-geostrophic turbulence in a simple special case. *Geophys. Astrophys. Fluid Dyn.*, **10**, 25–52.

Salmon, R. B., 1980: Baroclinic instability and geostrophic turbulence. *Geophys. Astrophys. Fluid Dyn.*, **10**, 167–211.

Sévellec, F., A. Colin de Verdière, and N. Kolodziejczyk, 2022: Estimation of horizontal turbulent diffusivity from deep Argo float displacements. *J. Phys. Oceanogr.*, **52**, 1509–1529.

Sévellec, F., A. Colin de Verdière, and N. Kolodziejczyk, 2024: Global observations of deep ocean kinetic energy transfers. *J. Phys. Oceanogr.*, **54**, 1633–1654.

Sévellec, F., and T. Huck, 2015: Theoretical investigation of the atlantic multidecadal oscillation. *J. Phys. Oceanogr.*, **45**, 2189–2208.

Sévellec, F., and T. Huck, 2016: Geostrophic closure of the zonally-averaged atlantic meridional overturning circulation. *J. Phys. Oceanogr.*, **46**, 895–917.

Sévellec, F., T. Huck, and M. Ben Jelloul, 2006: On the mechanism of centennial thermohaline oscillations. *J. Mar. Res.*, **64**, 355–392.

Sévellec, F., N. Kolodziejczyk, Q. Jamet, and A. Colin de Verdière, 2025a: Global observations of eddy-mean flow interactions at the ocean surface and in the deep ocean. *J. Phys. Oceanogr.*, **55**, 1569–1590.

Sévellec, F., N. Kolodziejczyk, and E. Portela, 2025b: Turbulent isopycnal mixing dominates thermohaline transformations of intermediate ocean waters. *Nat. Commun.*, **16**, 9838.

Sévellec, F., A. Naveira Garabato, and T. Huck, 2021: Damping of climate-scale oceanic variability by mesoscale eddy turbulence. *J. Phys. Oceanogr.*, **51**, 491–503.

Small, R. J., and Coauthors, 2008: Air-sea interaction over ocean fronts and eddies. *Dyn. Atmos. Oceans*, **45**, 274–319.

Starr, V. P., 1968: Physics of negative viscosity. *McGraw-Hill Book Company, New York*, pp. 256.

Talley, L. D., G. L. Pickard, W. J. Emery, and J. H. Swift, 2011: Descriptive physical oceanography: An introduction (sixth edition). *Elsevier*, 560 pp.

Taylor, G. I., 1921: Diffusion by continuous movements. *Proc. London Math. Soc.*, **20**, 196–212.

Tomita, H., K. Kunio, K. Masahisa, and H. Tsutomu, 2021: Advances in the estimation of global surface net heat flux based on satellite observation: J-ofuro3 v1.1. *Front. Mar. Sci.*, **8**, 612 361.

von Schuckmann, K., and Coauthors, 2023: Heat stored in the Earth system 1960–2020: where does the energy go? *Earth Syst. Sci. Data*, **15**, 1675–1709.

Walin, G., 1982: On the relation between sea-surface heat flow and thermal circulation in the ocean. *Tellus*, **34**, 187–195.

Wunsch, C., 2011: The decadal mean ocean circulation and Sverdrup balance. *J. Mar. Res.*, **69**, 417–434.

Yan, X., D. Kang, E. N. Curchitser, and C. Pang, 2019: Energetics of eddy-mean flow interactions along the western boundary currents in the North Pacific. *J. Phys. Oceanogr.*, **49**, 789–810.

Zika, J. D., M. H. England, and W. P. Sijp, 2012: The ocean circulation in thermohaline coordinates. *J. Phys. Oceanogr.*, **42**, 708–724.

Zika, J. D., N. Skliris, A. J. G. Nurser, S. A. Josey, L. Mudryk, F. Laliberté, and R. Marsh, 2015: Maintenance and broadening of the ocean's salinity distribution by the water cycle. *J. Climate*, **28**, 9550–9560.